Evidence of Early Sarmatian volcanism in the Hrvatsko Zagorje Basin, Croatia: Mineralogical, geochemical and biostratigraphic approaches

ANITA GRIZELJ[1,✉], MONIKA MILOŠEVIĆ[1], MIRJANA MIKNIĆ[2],
VALENTINA HAJEK-TADESSE[1], KORALJKA BAKRAČ[1], INES GALOVIĆ[1],
LUKA BADURINA[3], TOMISLAV KUREČIĆ[1], LARA WACHA[1], BRANIMIR ŠEGVIĆ[3],
MARIO MATOŠEVIĆ[4], ANA ČAIĆ-JANKOVIĆ[1] and RADOVAN AVANIĆ[5]

[1]Croatian Geological Survey, Department of Geology, Sachsova 2, 10000 Zagreb, Croatia; ✉agrizelj@hgi-cgs.hr
[2]Bartolići 49, 10000 Zagreb, Croatia
[3]Department of Geosciences, Texas Tech University, 1200 Memorial Circle, Lubbock 79401 TX, USA
[4]INA – Industrija nafte d.d., Exploration & Production, Subsurface & Field Development, Exploration & Production Laboratory,
Lovinčićeva 4, 10000 Zagreb, Croatia
[5]Šipki 5, 10000 Zagreb, Croatia

Abstract: A bentonite clay layer is documented in the Sutla-II column in the Hrvatsko Zagorje Basin, which is a part of the south-western marginal belt of the Pannonian Basin System. The origin of the clay is attributed to the alteration of felsic to intermediate volcanic ash, which had been deposited between horizontally-laminated marls in a marine environment. Provenance analysis indicates that the marls were sourced from mixed, dominantly-felsic source rocks. Smectite present in the marls is therefore not solely of terrigenous origin and may also be related to volcanic ash weathering. Based on the fossil content, an inference has been made suggesting Early Sarmatian age of the sediment hosting the bentonite clay intercalation. The sedimentological and palaeontological data are in favour of the sedimentation at an inner shelf area marked by unstable palaeoenvironmental conditions. The upper part of the Sutla-II column was deposited in the high-energy environment consisting of impure biocalcarenite and biocalcrudite coupled with fossiliferous litharenite, which all mark an intensive redeposition of older rocks and fossiliferous formations. The bentonite clay likely originated from distant tephra sourced from volcanic eruptions, presumably located in the north-eastern part of the Carpathian–Pannonian Region during the post-rift stage of the back-arc Pannonian Basin System development.

Keywords: Carpathian–Pannonian Region, Sarmatian volcanism, bentonite, provenance, biostratigraphy

Introduction

The Carpathian–Pannonian Region (CPR), which is located in eastern Central Europe, is defined by a vast basinal area – the Pannonian Basin System (PBS) – formed in the back of an arcuate orogenic belt, i.e., the Carpathian Mts. (Fodor et al. 1999). During the Middle Miocene, volcanism was widespread in the CPR (Pécskay et al. 2006; Szakács et al. 2018; Rybár et al. 2019), providing a good correlation potential between volcaniclastic rocks and their alteration products. The latter stands for volcanic ash altered in a marine environment to form bentonite clays largely made of smectites (Chamley 1989; Weaver 1989).

The Croatian part of the PBS consists of the smaller Hrvatsko Zagorje Basin (HZB), which is the subject of this research, and the larger North Croatian Basin (NCB) (Fig. 1a,b). Numerous occurrences of volcanic and volcaniclastic rocks and their altered varieties dating from the Lower to Middle Miocene have been studied in the Croatian part of the PBS (Pamić 1997; Mandic et al. 2012; Marković 2017; Brlek et al.

2020; Gverić et al. 2020; Badurina et al. 2021; Marković et al. 2021; Pavelić et al. 2022). While pyroclastic rocks and bentonites are common in the Croatian part of the PBS's Middle Miocene, they are generally more common in the Badenian than in the Sarmatian (Pavelić & Kovačić 2018). Moreover, such significantly-reduced volcanic activity during the Sarmatian is characteristic of the post-rift stage of the PBS development (Pavelić & Kovačić 2018 and references therein). Several smaller volcanic occurrences are related to the HZB (Šimunić et al. 1981, 1982; Aničić & Juriša 1984, 1985; Braun 1991; Šimunić & Pamić 1993; Tibljaš et al. 2002; Avanić 2012; Avanić et al. 2015, 2021). In the Lower Miocene (Egerian–Eggenburgian) these were mainly andesite tuffs, tuffites, and bentonite clays, extending along the Periadriatic lineament fault zone (Šimunić et al. 1981, 1982; Aničić & Juriša 1984, 1985; Braun 1991; Šimunić & Pamić 1993; Pamić & Pécskay 1996; Pamić 1997; Tibljaš et al. 2002; Avanić 2012; Avanić et al. 2015, 2021). Bentonite clays within Badenian marine deposits are documented in the vicinity of the studied area (Braun 1991; Pamić & Pécskay 1996; Marković 2002). Although

volcanic and volcaniclastic rocks in the Sarmatian have here-tofore not been found in the HZB, their occurrence is, how-ever, reported within the CPR (Pécskay et al. 1995, 2006; Rosu et al. 1997; Nagy & Kónya 2005; Püspöki et al. 2005, 2008; Seghedi et al. 2005; Harangi & Lenkey 2007; Kiss et al. 2010; Lexa et al. 2010; Seghedi & Downes 2011; Kovacs et al. 2013; Kovačić et al. 2015 a, b; Szakács et al. 2018; Mandic et al. 2019). During the Middle Miocene, the evolution of
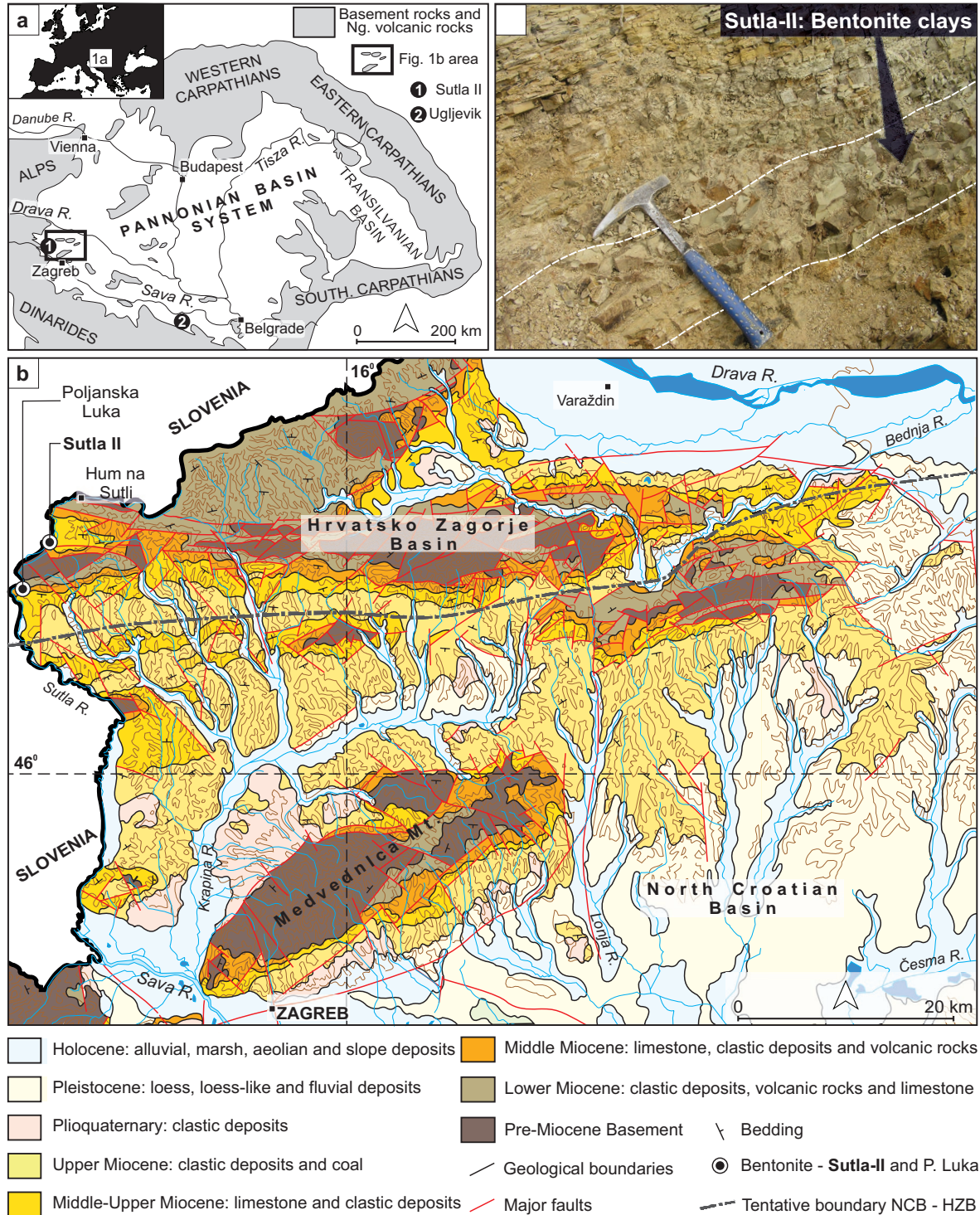

Fig. 1. a — Sketch map of the Pannonian Basin System area and surrounding mountain belts with the marked position of the investigated area; **b** — Simplified geological map of north-western Croatia with indicated positions of the Hrvatsko Zagorje Basin, the North Croatian Basin, and the position of the investigated Sutla-II site (map compiled after Hrvatski Geološki Institut (2009) and Pavelić & Kovačić (2018)); **c** — Investigated Middle Miocene (Sarmatian) deposits of Sutla-II containing a layer of bentonite clays.

the CPR was marked by subduction at the orogenic front, asthenosphere rising, and thinning of the crust in the back-arc region (Royden 1988; Konečný et al. 2002; Lexa et al. 2010). Volcanic activity was characterised by migration from west to east (Lexa et al. 2010; Szakács et al. 2018). Magmas that reached the surface were mainly of intermediate calc-alkaline and less felsic composition (Pécskay et al. 1995, 2006; Harangi & Lenkey 2007; Lexa et al. 2010). The felsic volcanic activity substantially diminished around 14–12 Ma and shifted to the Intra-Carpathian area (Pécskay et al. 1995, 2006; Szakács et al. 2018). At that time, andesite-composition activity was still producing large volumes of volcanic rocks in the Central Slovak Volcanic Field (Harangi & Lenkey 2007; Szakács et al. 2018). The intermediate calc-alkaline volcanism intensified with documented eruptions at several phases in the Apuseni Mts. in Romania, as well as along the Carpathians (Rosu et al. 1997, 2004; Konečný et al. 2002; Szakács et al. 2018).

This paper aims to determine the time sequence and key factors in the development of the Sarmatian sedimentary environment of the south-western marginal belt of the PBS. Furthermore, the article looks into the plausible relation with other parts of the Central Paratethys. The analysed bentonite clay has significant stratigraphic importance and provides valuable information about petrogenetic processes during the back-arc basin formation. For that reason, a complex geological approach combining mineralogy, geochemistry, sedimentology, and palaeontology was utilized to reach the set goals. Finally, the composition of the studied bentonite was compared with that of Badenian clay from the former clay pit of Poljanska Luka (Northern Croatia; Braun 1991; Gverić et al. 2020) and Early Sarmatian tuffaceous clay from the Ugljevik column (NE Bosnia and Herzegovina, Fig. 1a; Mandic et al. 2019; Badurina et al. 2021) to assess plausible correlations on a regional scale.

Geological setting

The investigated Sutla-II outcrop is located in the north-western part of Croatia near the Sutla river and the state border with Slovenia. It is a part of the south-western marginal belt of the PBS (Fig. 1a) known as the HZB (Pavelić 2001; Pavelić & Kovačić 2018) (Fig. 1b). Along with the Alpine, Carpathian, and Dinaric Mountain belts, the PBS was once a part of the CPR (Handy et al. 2015). During the Miocene in the CPR, volcanic activity was closely related to geodynamic evolution and the formation of the Mediterranean back-arc basin by subduction of the European Plate beneath the African (Apulian) Plate (Fodor et al. 1999; Csontos et al. 2002). The first (syn-rift) stage of basin development was characterised by the asthenosphere rising, tectonic thinning of the crust, and isostatic subsidence, while the second (post-rift) stage was marked by basin subsidence caused by the cooling of the lithosphere (Royden 1988; Tari et al. 1992). In the south-western part of the PBS, the first stage lasted from the Ottnangian to the Middle Badenian, while the second stage extended from

the Late Badenian to the end of the Quaternary (Pavelić 2001; Pavelić & Kovačić 2018).

Palaeogeographically, the PBS belongs to the Central Paratethys realm, a sedimentary area that lost its connection with the world ocean several times and later re-established itself during the Miocene (Steininger et al. 1988; Rögl 1996; Harzhauser & Piller 2007; Kováč et al. 2017, 2018).

During the Early Miocene in the area of northern Croatia, two basins with a different history of deposition were formed. The smaller HZB covered the area of the north-western part Croatia that extended westward to eastern Slovenia (Fig. 1b), and the other, larger NCB covered almost the entire remaining of what is now northern Croatia (Pavelić 2001; Pavelić & Kovačić 2018) (Fig. 1b). There were significant differences in deposition environments between the basins in the Early Miocene. The HZB was characterised by brackish and marine deposition in the Egerian to Late Ottnangian, as well as throughout the whole Middle Miocene, except for the Early Badenian. During the Late Ottnangian to Early Badenian, deposition was in a freshwater environment (Avanić 2012; Mandic et al. 2012; Avanić et al. 2021). Its evolution in the Early and Middle Miocene was strongly controlled by several phases of tectonic activity and accompanying volcanism (Avanić et al. 2021 and references therein). In the NCB, deposition began in a continental Ottnangian environment after a long-lasting emersion, which eventually progressed into marine deposition in the early and Middle Badenian and ended in the Pannonian (Pavelić 2001; Ćorić et al. 2009; Galović 2017; Brlek et al. 2018, 2020; Pavelić & Kovačić 2018; Marković et al. 2021; Kopecká et al. 2022).

Middle Miocene deposits cover a large area of northern Croatia (Fig. 1b), and their evolution is similar in both basins (HZB and NCB). While Upper Badenian sediments were formed in a marine environment, Sarmatian sediments are characterised as brackish or marine with reduced salinity (Vrsaljko 1999; Pavelić et al. 2003; Galović & Bajraktarević 2006; Vrsaljko et al. 2006; Grizelj et al. 2020). During the Sarmatian, sedimentation took place in the two different deposition environments: the shallow water environment, represented by conglomerates, calcarenites, and limestones, and a deeper marine environment, characterised by horizontally laminated pelitic sedimentary rocks (Pavelić et al. 2003; Avanić et al. 2018; Pavelić & Kovačić 2018).

Materials and methods

Fieldwork

Field research was carried out at outcrops located along the road near the Sutla River and border with Slovenia (Fig. 1b). A geological column was recorded and measured in detail, sedimentologically described, and photographs were taken. A total of 25 samples (marked in Fig. 2) were collected from exposed sediments for mineralogical, petrographic, chemical, and palaeontological analyses. The tuffaceous clay sample
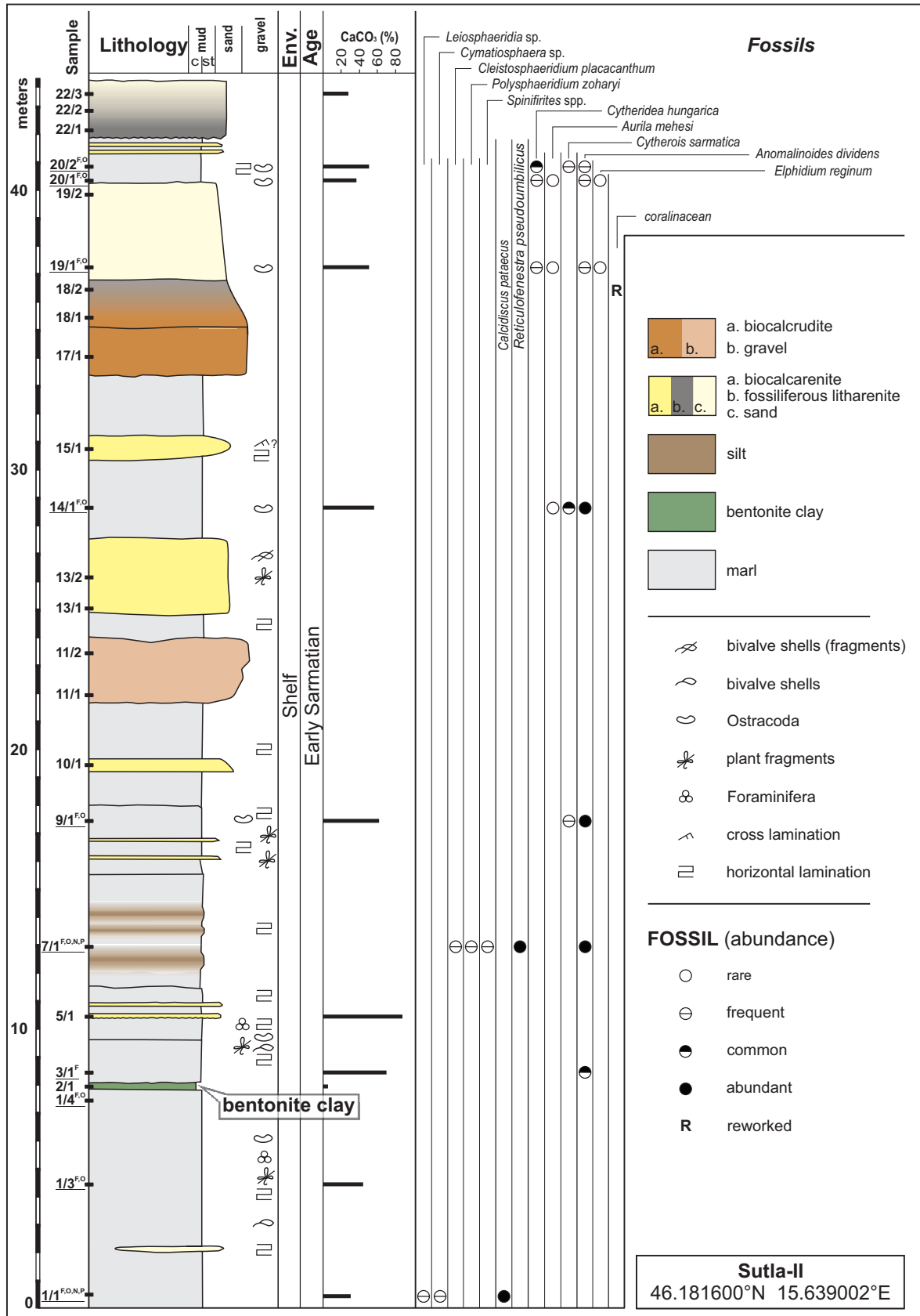
Fig. 2. Geological column Sutla-II (Sut-II) with sample positions (palaeontological analyses were made on the underlined samples: F – foraminifera, O – ostracods, N – calcareous nannoplankton, P – palynofacies and palynomorphs), CaCO₃ content, fossils distribution with palaeoenvironment interpretation.

from Ugljevik was acquired from the archives of Texas Tech Department of Geosciences.

Mineralogical and geochemical analysis

X-ray diffraction analysis (XRD) on whole-rock and oriented clay fractions was performed on seven representative samples. Clay fraction measurements included sample preparation consisting of carbonate dissolution using acetic acid with ammonium acetate (1 mol dm^{-3}) pH 5 buffer (Jackson 1956) and separation of the fraction below 2 μm in size by centrifugation (Krumm 1994). XRD patterns were recorded using a PANalytical vertical goniometer (type X'Pert) equipped with a Cu-tube under the following experimental conditions: 45 kV, 40 mA, PW 3018/00 PIXcel detector, primary beam divergence 1/4° and continuous scanning (step 0.02° 2θ/s). The clay fraction was analysed according to Starkey et al. (1984) and Moore & Reynolds (1997). The preparation of treated samples included: (a) air drying, (b) ethylene-glycol solvation, (c) saturation with K^+, (d) saturation with Mg^{2+}, (e) Mg^{2+} saturation and ethylene-glycol solvation, (f) K^+ saturation and ethylene-glycol solvation, (g) Mg^{2+} saturation and glycerol solvation, (h) K^+ saturation and dimethyl sulfoxide (DMSO) solvation, and (i) heating more than 30 min to 400 °C and 550 °C. According to the procedure described by Greene-Kelly (1953, 1955) the type of smectite was determined on the bentonite clay sample. This method involved saturating the sample with Li^+ (using 3N LiCl), then heating to 200 °C, and afterwards treatment with glycerol for 24 hours. XRD traces interpretation was carried out using the PANalytical software package and International Centre for Diffraction Data database (2021). The whole-rock fraction quantitative analysis was performed according to Schultz (1964). The amount of opal-CT was obtained as a residue up to 100 %, while the amount of aragonite and calcite was obtained using chemical analysis and XRD patterns. The composition of clay minerals in the clay fraction was estimated using the method of Biscaye (1965). Bentonite clay (Sut-II 2/1) was additionally studied and documented using a scanning electron microscope (SEM) JEOL JSM-6510 LV SEM (INA – Industrija nafte d.d.).

The mineralogical composition of heavy and light minerals fractions (HMF and LMF, respectively) was analysed in three sandy samples. These analyses were performed using the 0.09–0.160 mm fraction after removing the carbonates using HCl (4 %). The HMF and LMF were separated using $CHBr_3$ ($\rho = 2.90$ gcm^{-3}). The qualitative and quantitative composition of HMF and LMF were obtained by identifying up to 300 grains per fraction under a polarising microscope (Mange & Maurer 1992).

A set of ten thin sections of lithified rock samples were prepared to determine their biogenic and petrographic characteristics.

The content of calcium carbonate (% $CaCO_3$) in 11 samples was determined by an SCM1 calcimeter according to Scheibler's method (Behr Labor-Technik 2017).

A set of seven samples analysed by XRD was analysed at the Activation Laboratories Ltd (Vancouver BC, Canada) using a combination of inductively-coupled plasma–optical emission spectrometry (ICP-OES) and inductively coupled plasma–mass spectrometry (ICP-MS) methods to unveil their major and trace elements chemistry. Also, bentonite and tuffaceous clay (Sut-II 2/1 and Ugljevik-1) clay fractions were analysed at Texas Tech GeoAnalytical Laboratory using the laser ablation–inductively-coupled plasma–mass spectrometry (LA-ICP-MS) following the procedure described by Badurina & Šegvić (2022).

Provenance analysis relied on trace elements ratios (La/Co, Th/Co, Th/Sc, $Eu/Eu^* = Eu_N/(Sm_N \times Gd_N)^{1/2}$, LREE/HREE), ternary diagrams La–Th–Sc (Taylor & McLennan 1985; Bhatia & Crook 1986; Cullers 1994) and diagrams based on elemental ratios proposed by Winchester & Floyd (1977) and Gorton & Schandl (2000). Al-normalized enrichment factors as an estimate of trace metal enrichment were calculated for Mo, Ni, U as $X_{EF} = (X_{sample}/Al_{sample})/(X_{UCC}/Al_{UCC})$ (Algeo & Li 2020 and references therein), UCC values from Taylor & McLennan (1985).

Palaeontological analyses

Palaeontological analyses were performed on archived material prepared by standard laboratory methods.

Micropalaeontological analyses were performed on ten samples. About 100 g of sediment per sample were soaked with diluted hydrogen peroxide for disintegration, washed through the sieves (0.75, 0.25, 0.09 and 0.063 mm), and dried at room temperature. Fossil remains of ostracods and foraminifera were hand-picked from each dried residue and inspected under a binocular microscope (WILD M3Z) and Zeiss stereomicroscope. Only qualitative analysis was done due to the large number of reworked microfossils, which made differentiation of autochthonous and allochthonous specimens very difficult. Also, poor preservation, which was likely due to the erosion and reworking, as well as an insufficient number of specimens, made quantitative analyses virtually impossible. The estimation of foraminiferal and ostracod abundances is shown in Electronic Supplements 4 and 5.

For the calcareous nannofossil analyses, the standard preparation method of the Croatian Geological Survey was applied (Galović & Bajraktarević 2006). Approximately 1 cm^3 of the sediment was placed in a beaker and treated with H_2O_2 (30 %). Sediments were then rinsed several times with distilled water. Dense samples were put in an ultrasonic bath for approximately 15 s to disaggregate. The standard smear slide preparation technique and the light microscope (LM) were used for the analysis of calcareous nannofossils. The LM slides were mounted with Canada balsam on a hot plate and examined using a BH2 Olympus LM.

Palynological analyses were carried out on two marl samples. Standard palynological processing techniques were used to extract the organic matter (e.g., Moore et al. 1991; Wood et al. 1996). For palynofacies analysis, slides were mounted in

glycerine, and for palynomorphs analysis in silicon oil. Microscopic analyses were performed using the Olympus BH2 and Leica DM2500 transmitted light microscope. Photomicrographs were taken using an AmScopeTM camera adapter connected to the AmScope v.3.7 camera software and a Leica MC190 HD camera connected to the Leica LAS EZ software. For the environmental interpretation, only qualitative palynofacies analyses were done because of the small amount and poor preservation of organic matter within the samples. Components were grouped according to the classifications proposed by Tyson (1995).

Fossil remains were also determined from thin-section samples and photo-documented under the polarised microscope Zeiss AXIOLAB 5. Selected calcareous nannofossil, foraminiferal, and ostracod species were studied and documented using the scanning electron microscopes (SEM) JEOL JSM-6510 LV SEM (INA – Industrija nafte d.d.) and JEOL JSM-35CF (Croatian Geological Survey).

Other fossil remains, such as the fragments of echinoderms, gastropods, bivalves, bryozoans, corallinaceans, and fish remains, were noted but not determined.

All micropalaeontological samples, organic residues, and palynological slides are currently stored at the Archives of the Department of Geology, Croatian Geological Survey, Zagreb, Croatia.

Results

The lithostratigraphic column Sutla-II and the mineralogical content

The lower part of the Sutla-II lithostratigraphic column is represented by marls and a bentonite clay layer, while the upper part is composed of sands, biocalcarenites, biocalcirudites, and marls. A detailed geological column is shown in Fig. 2.

The lower part (up to 21.5 m) comprises marls with rare 1–3 cm thick interlayers of silts or sands (Fig. 2). It begins with 7.8 m thick horizontally laminated to thin-layered marls, containing a 1–2 cm thick interlayer of sand in the third meter and numerous fragments of flora and bivalve moulds with sporadically-preserved shells. The 30 cm thick bentonite clay layer is intercalated within this marl interval. The bentonite is light grey homogeneous, and structureless with calcareous infiltrations (Fig. 1c). It is dominated by 14 Å clay minerals (60–70 %). In addition to them, it contains opal-CT (30 %) and calcite (0–10 %), while quartz is present in amounts that do not exceed 1 %. The same mineral components were determined in the clay fraction. Additional tests to identify the type of smectite minerals (Greene-Kelly 1953, 1955) unveiled a dioctahedral nature of smectite (i.e., montmorillonite; Fig. 3a). Figure 3b shows the honeycomb structure of montmorillonite. In the greater than 6.3 µm fraction, very small amounts of calcite, plagioclase, apatite, zircon, biotite, and ilmenite were detected by SEM and/or optical microscope. Figure 3c and 3d

outline authigenic montmorillonite overgrowths over plagioclase, calcite, and calcareous nannoplankton.

The lower and upper boundaries of the bentonite layer are sharp and flat. On top of it, horizontally-laminated to layered marls are exposed, containing rare interlayers of silt, sand, and biocalcarenite, similar to the first interval. These marls contain fossil remains like foraminifera and ostracods. Dominant minerals in all analysed marl samples are calcite (30–58 %) and clay minerals (30–48 %), while quartz is present in smaller quantities (6–17 %), as seen from XRD traces (Table 1). In addition to listed minerals, the Sut-II 1/3 sample contains cristobalite (4 %), opal-CT (12 %), and aragonite (14 %). In contrast, the sample Sut-II 20/2 has only a small amount of dolomite (5 %). Clay minerals with a diffraction maximum at 14 Å and 10 Å were present in all samples, while only three samples (Sut-II 3/1, Sut-II 7/1, and Sut-II 9/1) contained 7 Å diffraction maximum clay minerals (Table 1). In the clay fraction of these samples, smectites and illite are the most common (Table 1). Quartz and kaolinite, which do not intercalate with DMSO, are regularly present in small quantities. At the same time, chlorite is present in very small quantities in most samples. Kaolinite, which forms intercalation compounds with DMSO, is present in a very small amount in samples Sut-II 1/3 and Sut-II 3/1, and possibly also in the Sut-II 7/1 sample (Table 1). Opal-CT appears only in the Sut-II 1/3 sample.

The upper part of the column starts with 2.5 m of extremely chaotic sediments, whose grain size varies from pelite to gravel. The next interval consists of marls, followed by sandstones determined as impure biocalcarenite or fossiliferous litharenite and conglomerate (impure biocalcrudite) (Figs. 2 and 4). The impure biocalcarenite is medium to poorly-sorted, as well as fine- to medium-grained. It contains fossil carbonate and siliciclastic detritus with microsparite cement. Siliciclastic detritus consists predominantly of quartz and less of feldspars, mica, glauconite, fragments of quartzite, cherts, and volcanic particles. The fossil carbonate detritus predominantly consists of corallinacean fragments and a smaller number of benthic foraminifera, bryozoans, and fragments of echinoids and molluscs. Redeposited ooids, proto-ooids, aggregates, and oncoids were also recognised within the thin sections (Fig. 4). The impure biocalcrudite has almost the same composition as the impure biocalcarenite, but a larger grain size. Fossiliferous litharenite contains the same components as impure biocalcarenite, but has a significantly higher siliciclastic detritus and limestone fragments content than the fossil fragments. In the upper part of the column (samples Sut-II 19/1 and Sut-II 22/3), there are poorly-sorted silty sands from which the mineral content of LMF and HMF was analysed (Electronic Supplement 1). The results show that the dominant compounds in the LMF are quartz (65–74 %) and lithic fragments (15–29 %), while K-feldspars are less abundant (5–10 %) (Electronic Supplement 1). In all samples, a tiny amount of muscovite is present as well. Angular quartz grains with undulatory extinction predominate compared to those with uniform extinction. K-feldspar grains are usually highly-altered, while fresh grains

are rare. The most common rock fragments are tuffites and cherts, while quartzite-type particles and shists are rare. Among the HMF, translucent minerals dominate (59–91 %). Additionally, opaque minerals (8–38 %) and chlorite (1–4 %) appear in all analysed samples, while dolomite is present in a quantity of 1–2 % only in samples Sut-II 11/1 and Sut-II

19/1. Garnet is the most abundant translucent heavy mineral in all samples (Electronic Supplement 1). Its quantity ranges from 68 to 85 %. Tourmaline, rutile, zircon, kyanite, and staurolite are less abundant. The epidote group of minerals occurs in very small quantities in all samples, while apatite and titanite are present only in the Sut-II 19/1 sample. The colour
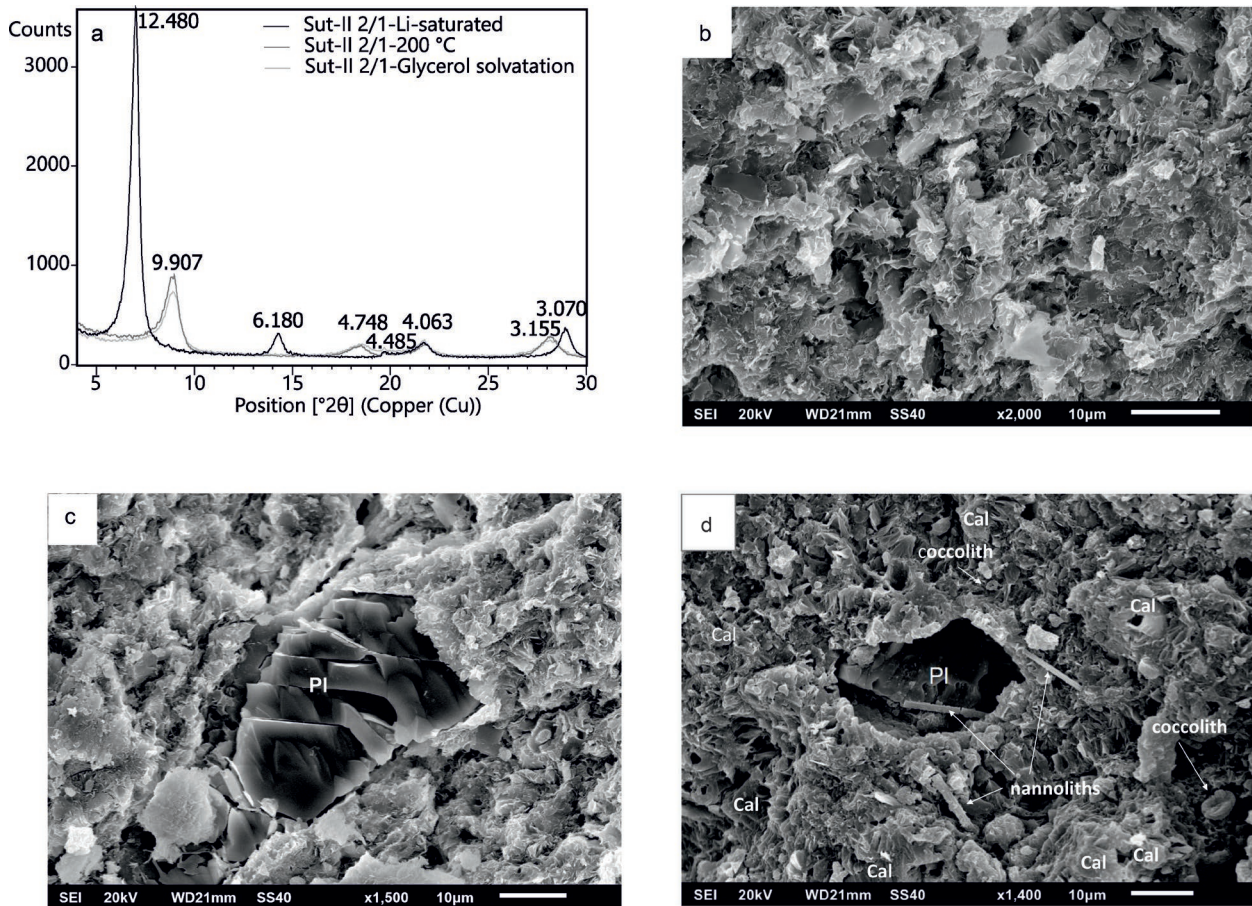

Fig. 3. Bentonite clay (Sut-II 2/1): **a** — XRD patterns with d-values (Å) after Greens-Kelly test; **b** — SEM image of montmorillonite; **c** — SEM image of montmorillonite and plagioclase; **d** — SEM images of montmorillonite, plagioclase (Pl), calcite (Cal), nannoliths and calcareous nannoplankton.

Table 1: Quantitative mineral composition of the whole-rock samples and semi-quantitative mineral composition of the <2 μm fraction of insoluble rock residue obtained by XRPD. Clay mineral content was determined in the <2 μm fraction of insoluble rock residue. Qtz – quartz, Cri – cristobalite, Cal – calcite, Arg – aragonite, Dol – dolomite, 14Å, 10Å, 7Å – type of clay minerals, Y – present in sample, CM – clay minerals, Sme – smectite, Ill – illite, Kln – kaolinite which does not intercalate with DMSO, KlnD – kaolinite which forms intercalation compounds with DMSO, Chl – chlorite, XXX – dominant (>50 %), XX – abundant (20–50 %), X – subordinate (1–20 %), tr – traces (<1 %), ? – mineral is probably present in the sample, but cannot be confirmed with certainty because of low content and/or overlapping of diffraction maximums.

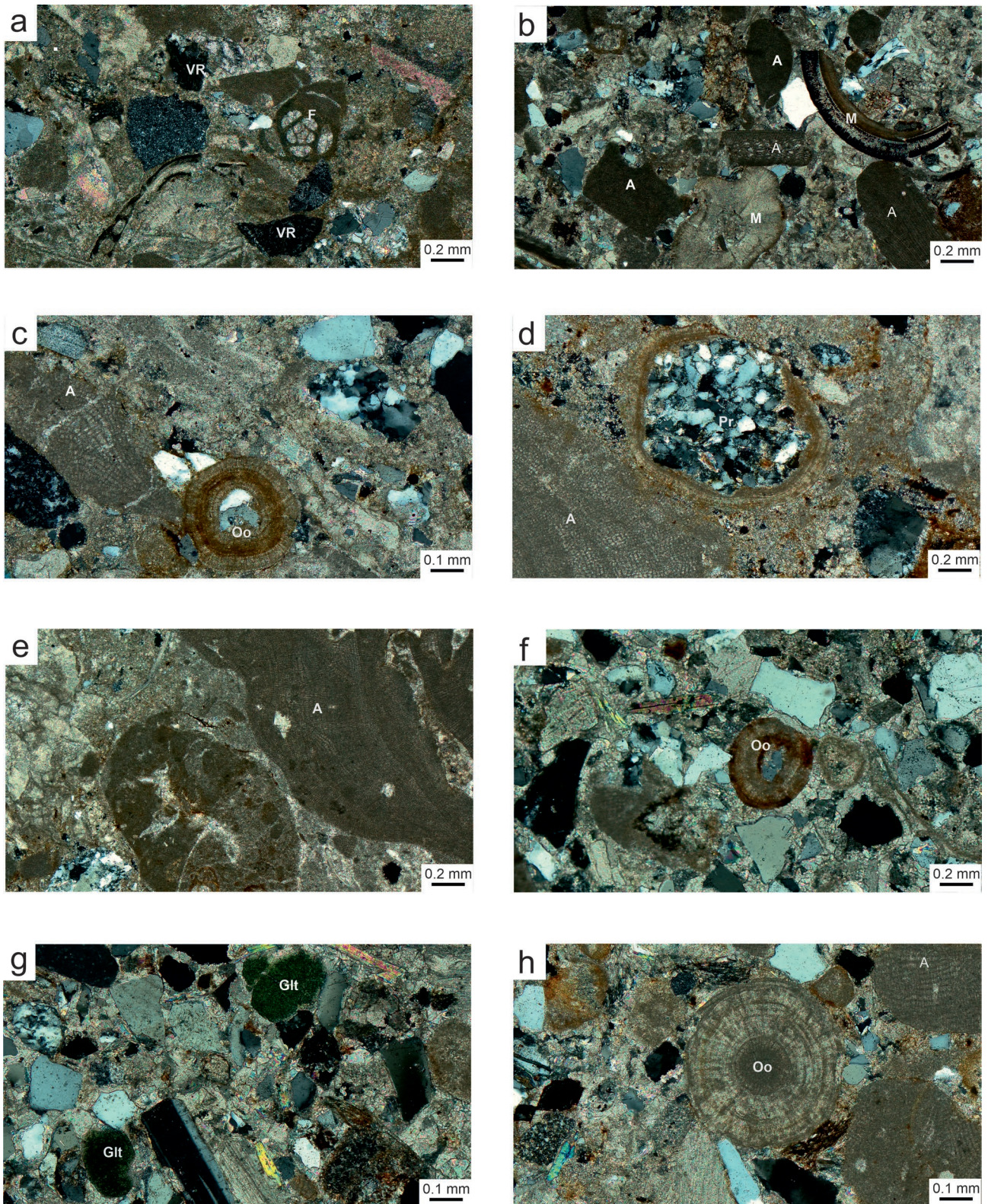| SAMPLE	global rock										fraction <2μm						
	Qtz	Cri	opal-CT	Cal	Arg	Dol	14 Å	10 Å	7 Å	CM	Sme	Ill	Kln	KlnD	Chl	opal-CT	Qtz
Sut-II 1/3	10	4	12	30	14		Y	Y		30	XXX	XX	X	tr		X	X
Sut-II 2/1	tr		30	0-10			Y			60-70	XXX					XX	tr
Sut-II 3/1	6			55			Y	Y	Y	39	XXX	XX	X	tr	tr		X
Sut-II 7/1	17			35			Y	Y	Y	48	XXX	XX	X	?	tr		X
Sut-II 9/1	6			58			Y	Y	Y	36	XXX	XX	X		tr		X
Sut-II 14/1	10			48			Y	Y		42	XXX	XX	X				X
Sut-II 20/2	16			39		5	Y	Y		40	XXX	XX	X		tr		X

Fig. 4. Images of thin sections of: **a** — impure biocalcarenite, Sut-II 10/1; **b** — impure biocalcarenite, Sut-II 13/2; **c** — impure biocalcarenite, Sut-II 15/1; **d** — impure biocalcrudite, Sut-II 17/1; **e** — impure biocalcrudite, Sut-II 18/1; **f, g** — fossiliferous litharenite, Sut-II 18/2; **h** — fossiliferous litharenite, Sut-II 22/1, using a polarising microscope (analyser on). VR – volcanic rock, F – Foraminifera, M – fragment of Mollusca, A – Corallinacea, Pr – proto-ooide, Oo – ooide, Glt – glauconite.

of the garnets is transparent to pale pink. Corroded and irregu-larly-broken garnet grains prevail, while subhedral grains are rare. Tourmaline is light brown to dark brown. Among tourma-lines, irregular grains are common, although subhedral grains also occur. Rutile is orange to dark red and often has irregu-larly-shaped and corroded grains. Zircons are present as sub-rounded or subhedral grains. Staurolite is yellow to pale yellow. Both staurolite and kyanite are present as slightly-corroded grains. Epidotes are yellow-green and presented as corroded, weathered grains.

Geochemistry

The content of $CaCO_3$ measured by SCM1 calcimeter varies from 0–11 % in bentonite clay, 36–58 % in marls, and up to 85 % in impure biocalcarenite as shown in Fig. 2. The whole-rock sample geochemistry, which includes major and trace elements, is provided in Electronic Supplement 2. Chemical analysis showed that marly rocks are largely made of SiO_2 (22.89–38.98 %), CaO (20.82–32.86 %), LOI (21.8–31.10 %), Al_2O_3 (7.13–10.25 %), and minor amounts of $Fe_2O_3(T)$ (2.87–3.31 %), K_2O (1.10–1.88 %), MgO (0.83–2.31 %), TiO_2 (0.18–0.98 %), Na_2O (0.15–0.41 %), P_2O_5 (0.266–0.477 %) and MnO (0.044–0.055 %). Conversely, the bentonite clay (Sut-II 1/2) predominantly contains SiO_2 (60.69 %), Al_2O_3 (10.59 %), LOI (17.55 %), CaO (7.96 %), and a smaller amount of $Fe_2O_3(T)$ (1.46 %), MgO (1.25 %), K_2O (0.24 %), TiO_2 (0.162 %), Na_2O (0.12 %), P_2O_5 (0.09 %) and MnO (0.024 %).

The clay fraction geochemistry of Sut-II 2/1 and Ugljevik-1 is provided in Electronic Supplement 3.

Trace element concentrations of marls normalised to Upper Continental Crust (UCC) (Taylor & McLennan 1985) and primitive mantle (Sun & McDonough 1989) for bentonite clay are given in Fig. 5 a and b. Marls are characterised by positive anomalies of U and Sr, which may be related to higher contents of smectite and carbonates, respectively (Fig. 5a). The diagram in Fig. 5b shows higher values of Rb in Ugljevik-1 clay fraction than in Sut-II 2/1 bentonite clay and their clay fraction. In contrast, the other elements show similar elemen-tal distributions. Pronounced negative Ti and positive U and Th anomalies are likely related to the presence of accessory phases. Moreover, light rare earth elements (LREE) display a consistent enrichment relative to heavy rare earth elements (HREE). The same can be inferred from the chondrite nor-malised values of Taylor & McLennan (1985) for all studied samples (Fig. 5c, d), which is further indicated by the LREE/HREE ratio ranging from 7.3 to 8.1 in marls. For the bento-nite clay of Sut-II 2/1, it is 13.49 (Electronic Supplement 2). All analysed samples also show negative Eu-anomalies, ran-ging from 0.54–0.63 (Electronic Supplement 2).

Microfossil analyses

The lowest part of the studied column (samples Sut-II 1/1, Sut-II 1/3, Sut-II 1/4) is represented by a poorly-preserved foraminiferal assemblage composed of small-sized specimens. A high abundance of epiphytic taxa and a low number of infaunal taxa and infaunal/epifaunal taxa are the main charac-teristics of the foraminiferal assemblage. Keeled elphidiids (*Elphidium joukovi*, *E. grilli*, *E. josephinum*, *E. koberi* (Fig. 6e), *E. subumbilicatum*, *E. macellum*, *E. fichtelianum*) are domi-nant. Non-keeled elphidiids (*Elphidium hauerinum* (Fig. 6c), *Elphidiella serena*) are also present, while molds of miliolids (*Varidentella reussi*, *Cycloforina badenensis*, *Pseudotri-loculina consobrina*) are abundant. Bolivinids (*Bolivina dila-tata*, *B. granensis*, *B. moldavica*, *B. moravica*, *B. pokornyi*, *B. pseudoplicata*, *B. saggitula*, *B. sarmatica*) together with small benthic foraminifera (*Asterigerinata mamilla*, *Biasteri-gerinata planorbis*, *Aubignyina* sp. (Fig. 6z), *Fissurina miro-novi*, *Nonion biporus*, *N. tumidulus*, *Neoconorbina terquemi*, *Porosononion martkobi*, *P. granosum*, *P.* cf. *aragviensis*) and reworked Badenian planktonic foraminifera are rare.

The first occurrence of *Anomalinoides dividens* (Fig. 6a, b) is recorded in sample Sut-II 3/1, accompanied by an impo-verished foraminiferal assemblage. Samples Sut-II 7/1 and Sut-II 9/1 are characterised by a practically monospecific assemblage of *Anomalinoides dividens*. Rare specimens from the lowermost samples (Sut-II 1/1, Sut-II 1/3, Sut-II 1/4) are also present, along with the sporadic occurrence of *Nodosaria dina*, *Ammonia pseudobeccarii*, and *Schackoinella impera-toria*. Reworked Badenian benthic (*Lenticulina* sp., *Pappina neudorfensis*, *Spirorutilus carinatus*, *Uvigerina brunnensis*, *Semivilvulina pectinata*, etc.) and planktonic (*Globigerina diplostoma*, *Trilobatus quadrilobatus*, *Globigerina bulloides*, *Globigerinella regularis*) foraminifera are minor components. All identified foraminiferal taxa are listed in Electronic Supplement 4.

The diversity of ostracods is generally low in samples taken from Sut-II 1/1 to Sut-II 1/9. Rare fossil valves are pre-sent, including both juvenile and a few adult specimens. The ostracod assemblages include thirteen different species, which belong to ten genera: *Aurila* cf. *angulata*, *Aurila* sp., *Amnicythere* sp., *Callistocythere postvallata*, *Callistocythere* cf. *egregia*, *Cytherois sarmatica*, *Cnestocythere* cf. *truncata*, *Euxinocythere* sp., *Miocyprideis* sp., *Hemicytheria* sp., *Xestoleberis fuscata*, *Leptocythere* sp., and *Loxoconcha* sp. (Fig. 7, Electronic Supplement 5).

Coccoliths of *Calcidiscus pataecus* (Fig. 6za, aa), *Holo-discolithus macroporus* (Fig. 6zb) and *Rhabdosphaera sicca* dominate in sample Sut-II 1/1 accompanied by *Coccolithus pelagicus*, *Cyclicargolithus floridanus*, *Discoaster deflandrei*, *Helicosphaera walbersdorfensis*, *Pontosphaera multipora*, *Reticulofenestra minuta*, *Syracosphaera clathrata* and rare ascidian spicules. Species richness and abundance decrease in sample Sut-II 2/1 where *Calcidiscus pataecus* prevails (Fig. 2). Blooms of *Reticulofenestra*, dominated by *R. pseudo-umbilicus* (Fig. 6ab) are found in sample Sut-II 7/1. Only index species which dominate in the assemblage are presented in Fig. 2 and Fig. 6za, zb; aa–ab.

Palynofacies from the lowermost marl (sample Sut-II 1/1) contains a relatively small amount of organic residue

dominated by palynomorphs, while partially-gelified phyto-clasts and resinite are also present (Fig. 8a). In addition to numerous conifer pollen (mainly *Pinus*), phycomas of prasi-nophytes *Leiosphaeridia* (Fig. 8c), *Hidasia*, *Cymatiosphaera*, and rare poorly-preserved cyst of dinoflagellate *Operculodi-nium* are also present. Palynofacies from the sample Sut-II 7/1 contains small quantities of the organic residue dominated by heterogeneous phytoclasts and palynomorphs (Fig. 8b). Palynomorphs are dominated by numerous conifer (mainly *Pinus* and, to a lesser extent *Taxodium*), deciduous tree pollen (*Carya*), and dinocysts *Operculodinium* sp. indet., *Cleistosphaeridium placacanthum*, *Polysphaeridium zoharyi*

(Fig. 8d), *Lingulodinium machaerophorum* (Fig. 8e), *Spini-ferites* spp. and *Spiniferites bentorii*. Relative abundances of significant palynomorphs are shown in Fig. 2.

In addition to the mentioned fossil assemblage, rare frag-ments of fish and echinoids, *Semseya lamellata,* and fragments of algae are also present. Framboidal pyrite and pyrite filling of foraminiferal chambers and palynomorphs (Fig. 8f) are notable characteristics of sample Sut-II 7/1.

In the upper part of the column, better preservation, burlier specimens, domination of epiphytic taxa and a higher portion of reworked species, are common attributes of the foramini-feral assemblage. In addition to the dominant *Anomalinoides*

□ Sut-II 1/3   ● Sut-II 2/1   ○ Sut-II 3/1   △ Sut-II 7/1   ◇ Sut-II 9/1   ▽ Sut-II 14/1   ⊠ Sut-II 20/2   ● Sut-II 2/1 [CF]   ● Ugljevik-1 [CF]
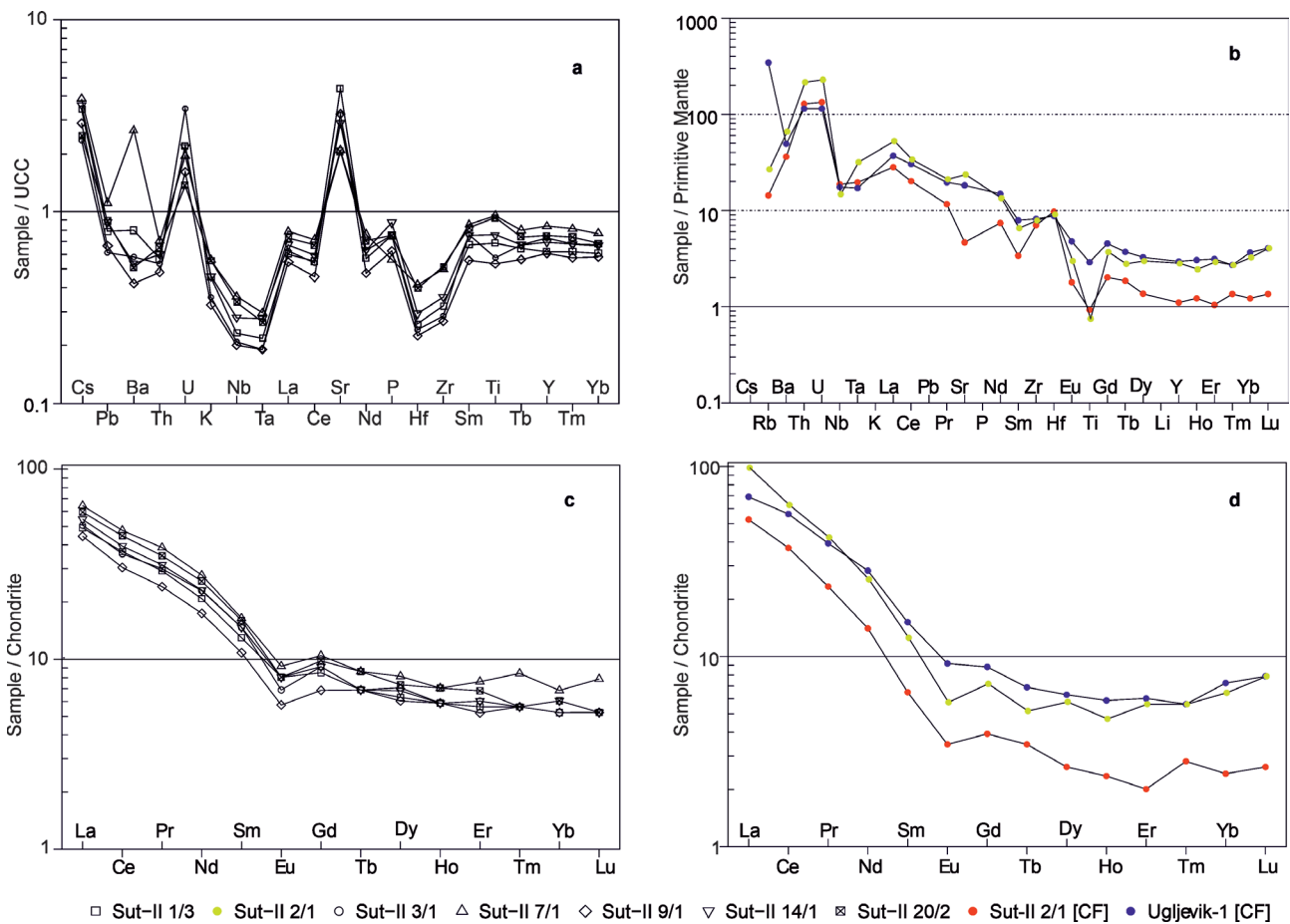
Fig. 5. a — The Upper Continental Crust (UCC) (Taylor & McLennan 1985); **b** — Primitive mantle (Sun & McDonough 1989) and **c, d** — The chondrite (Taylor & McLennan 1985) normalized plots for the analysed samples.

Fig. 6. Foraminiferal and nannoplankton assemblage from Sutla-II column. **a, b** – *Anomalinoides dividens* Łuczkowska, Sut-II 7/1; **c** – *Elphidium hauerinum* (d'Orbigny), Sut-II 1/1; **d** – *Elphidium reginum* (d'Orbigny), Sut-II 20/1; **e** – *Elphidium koberi* Tollmann, Sut-II 1/1; **f** – *Elphidium josephinum* (d'Orbigny), Sut-II 20/1; **g** – *Elphidium* ex. gr. *puscharovsky* Serova, Sut-II 3/1; **h** – *Elphidium fichtelianum* d'Orbigny, Sut-II 19/1; **i** – *Porosononion* cf. aragviensis (Dzhanelidze), Sut-II 1/1; **j** – *Borelis melo* (Fichtel & Moll), Sut-II 20/2; **k** – *Cycloforina contorta* (d'Orbigny), Sut-II 19/1; **l** – *Quinqueloculina akneriana* d'Orbigny, Sut- II 20/2; **m** – *Quinqueloculina hauerina* d'Orbigny, Sut-II 1/3; **n** – *Cycloforina stomata* Łuczkowska, SUT II 20/2; **o** – *Varidentella lantelaculata* (Venglinski), Sut-II 1/4; **p** – *Varidentella pseudocostata* (Venglinski), Sut-II 20/2; **r** – *Varidentella rosea* d'Orbigny, Sut-II 20/2; **s** – *Varidentella rotunda* (Gerke), Sut-II 20/2; **t** – *Varidentella sar-matica* (Karrer), Sut-II 20/2; **u** – *Articulina problema* Bogdanowicz, Sut-II 19/1; **v** – *Articulina* sp. Sut-II 20/1; **z** – *Aubignyna* sp. Sut-II 1/1; **za** – *Calcidiscus pataecus,* Sut-II 1/1; **zb** – *Holodiscolithus macroporus,* Sut-II 1/1; **aa** – *Calcidiscus pataecus,* Sut-II 2/1; **ab** – *Reticulofenestra pseudoumbilicus,* Sut-II 2/1.
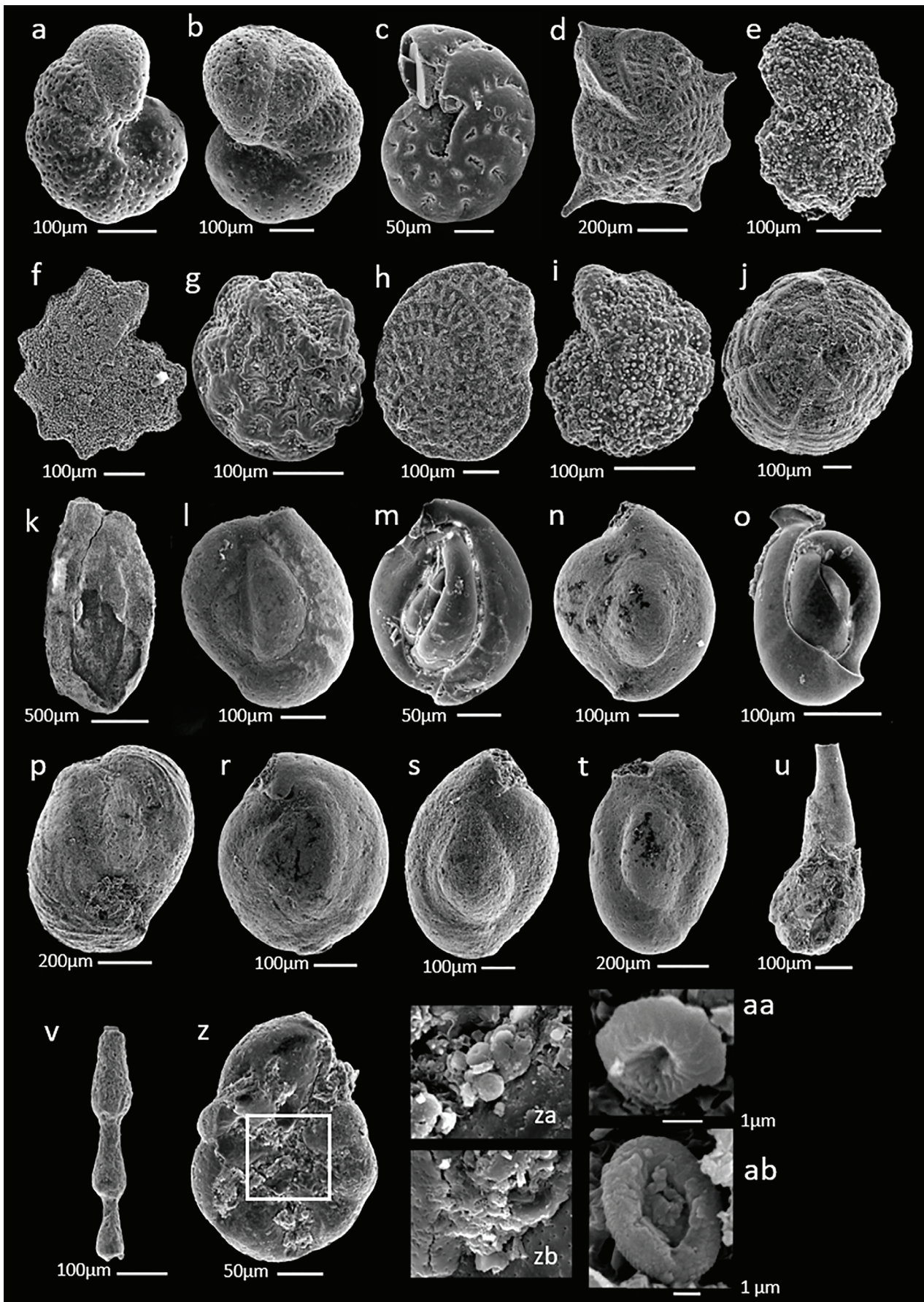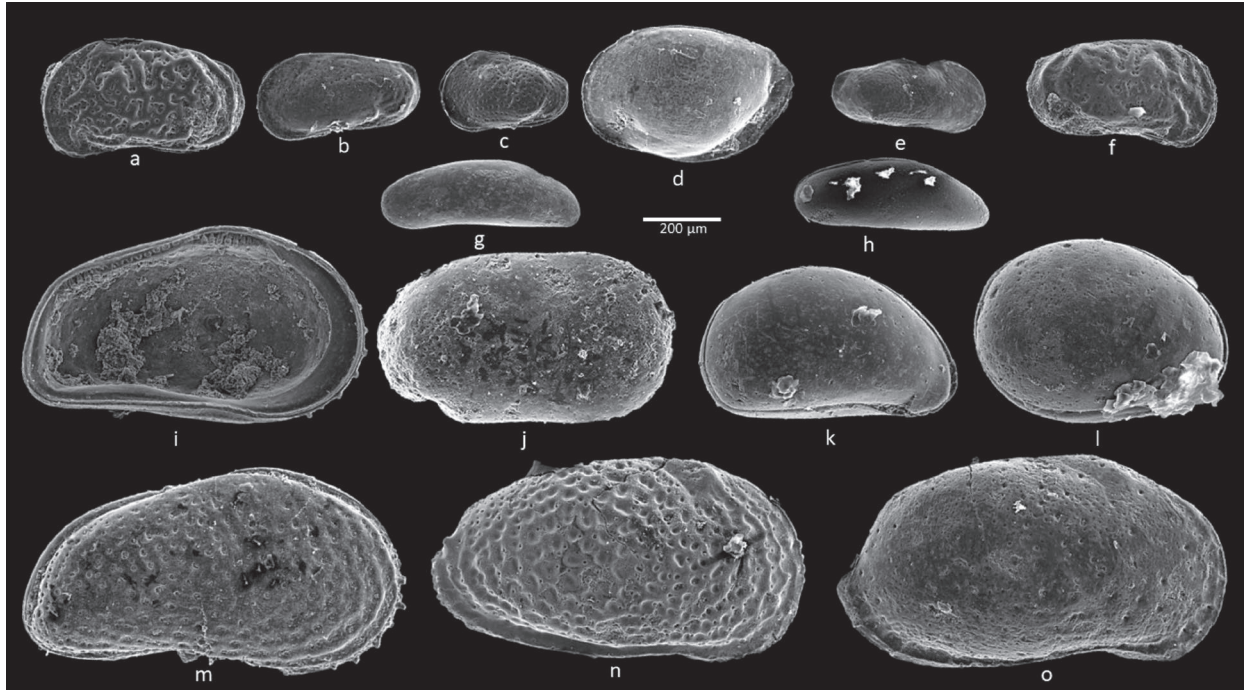
Fig. 7. Selected ostracods from the Sutla-II column. **a** – *Callistocythere* cf. *egregia*, lateral exterior view of LV, Sut-II 1/3; **b** – *Leptocythere* sp.*,* lateral exterior view of LV, Sut-II 14/1; **c** – *Euxinocythere* sp., lateral exterior view of LV, Sut-II 1/4; **d** – *Phlyctocythere pellucida* lateral exterior view of LV, Sut-II 14/1; **e** – *Aminocythere* sp., lateral exterior view of RV, Sut-II 1/1; **f** – *Callistocythere postvallata,* lateral exterior view of RV, Sut-II 1/4; **g, h** – *Cytherois sarmatica,* **g** – lateral exterior view of LV, Sut-II 14/1; **h** – C external view, Sut-II 14/1; **i** – *Cytheridea hungarica,* lateral interior view of LV, Sut-II 19/1; **j** – *Miocyprideis* sp., lateral exterior view of RV, Sut-II 20/1; **k** – *Xestoleberis fuscata,* C external view, Sut-II 14/1; **l** – *Xestoleberis* cf. *glaberescense,* C external view, Sut-II 20/2; **m** – *Cytheridea hungarica,* C external view, Sut-II 20/2; **n** – *Senesia* cf. *vadaszi,* lateral exterior view of RV, Sut-II 19/1; **o** – *Aurila mehesi,* lateral exterior view of RV, Sut-II 14/1. Explanation: RV: right valve; LV: left valve; C: carapace.
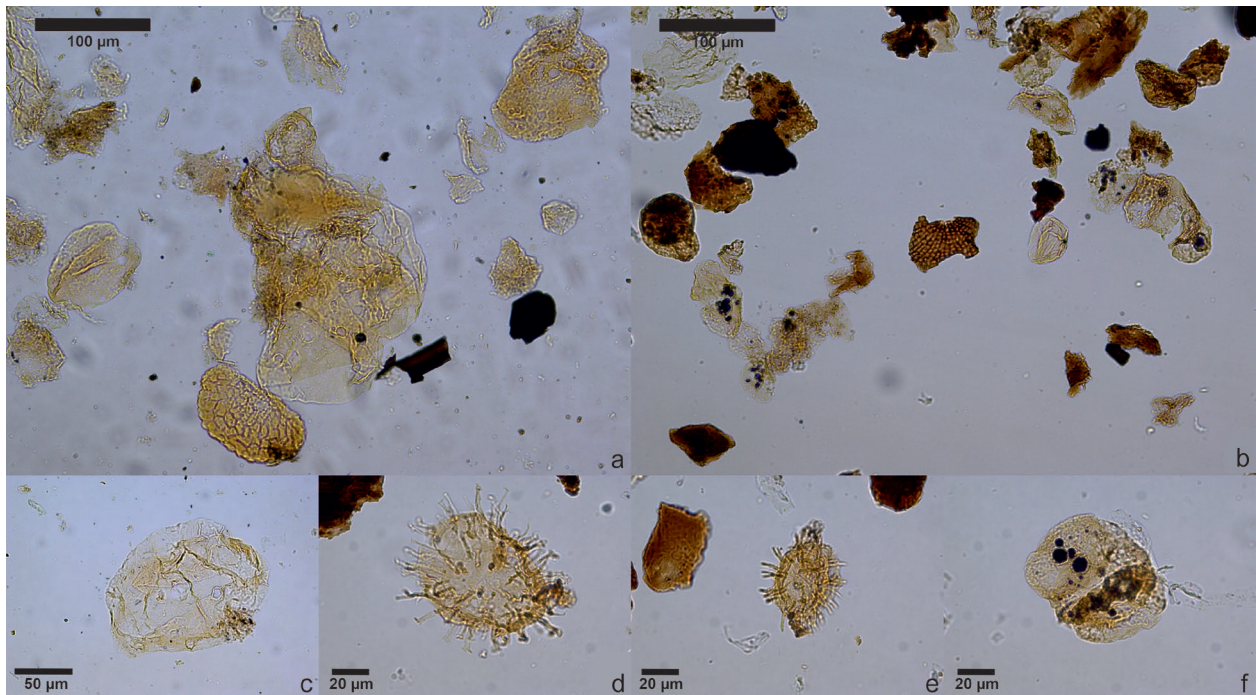

Fig. 8. Palynofacies and palynomorphs from the studied area: **a** – palynofacies, Sut-II 1/1; **b** – palynofacies, Sut-II 7/1; **c** – *Leiosphaeridia* sp., Sut-II 1/1; **d** – *Polysphaeridium zoharyi* (Rossignol 1962) Bujak et al. 1980, Sut-II 7/1; **e** – *Lingulodinium machaerophorum* (Deflandre and Cookson 1955) Wall 1967, Sut-II 7/1; **f** – *Pinus* sp. and pyrite grains, Sut-II 7/1.

dividens in sample Sut-II 14/1, nonionids are common (*Nonion tumidulus*, *N. bogdanowiczi*), while small benthic foraminifera (*Biasterigerinata planorbis*, *Neoconorbina terguemi*, *Lobatula lobatula*, *Bolivina dilatata*) together with elphidiids (*Elphidium* ex gr *puscharovsky* (Fig. 6g)*, E. macellum, E.* ex gr *flexuosum)* also occur. Abundant elphidiids (*Elphidium reginum* (Fig 6d), *Elphidium crispum*, *E. fichtelianum* (Fig. 6h), *E. grilli*, *E. macellum*, *E. flexuosum*, *E. obtusum*), dominate in the upper part of the column (samples Sut-II 19/1 and Sut-II 20/1). Miliolids (*Varidentella rotunda*, *V. rosea*, *V. sarmatica*, *Quinqueloculina akneriana*, *Q. hauerina*, *Articulina problema* (Fig. 6u) are also present. A significant number of reworked specimens is also a part of the assemblage. Except for the Badenian reworked species, some Paleogene species (*Pararotalia lithothamnica*, abraded nummulits, and operculinids) are present. In sample Sut-II 20/1, reworked specimens have a more significant portion than autochthonous, Sarmatian taxa. The topmost sample (Sut-II 20/2) contains prevailing miliolids (*Borelis melo* (Fig. 6j), *Varidentella reussi*, *V. rotunda* (Fig. 6s), *V. rosea* (Fig. 6r), *V. pseudocostata* (Fig. 6p)*, V. latelacunata*, *Cycloforina contorta*, *C. stomata*, *Quinqueloculina hauerina*, *Q. akneriana* (Fig. 6l)*,* fragments of *Articulina problema*. A similar foraminiferal assemblage as in previous samples (*Anomalinoides dividens*, *Elphidium* spp., *Ammonia pseudobeccarii*) is present.

From sample Sut-II 14/1 upwards, ostracods are more numerous and well-preserved. Adult valves and carapaces dominate within all samples. Twenty-five ostracod species have been identified in this part of the column. The maximum number of ostracod species (14) was reported in the Sut-II 19/1 sample. The samples Sut-II 20/1 and Sut-II 20/2 contain a relatively high number of ostracod species. The most numerous species are *Cytheridea hungarica*, *Aurila merita* and *Cytherois sarmatica*. Species *Aurila mehesi*, *Aurila* cf. *notata*, *Aurila* cf. *angulata*, *Aurila* sp.,*Amnicythere* sp., *Callistocythere* cf. *egregia*, *Cnestocythere* cf. *truncata*, *Miocyprideis* sp.*, Hemicytheria* sp., *Hemicytheria dacica dacica*, *Xestoleberis fuscata*, *Xestoleberis* cf. *glaberescense*, *Leptocythere* sp., *Loxocorniculum hastatum*, *Loxoconcha* sp., *Phlyctocythere pellucida*, *Paranesidea* sp., *Pachicaudites* sp., *Phlyctenophora* sp., *Senesia* cf. *cinctella,* and *Senesia* cf. *vadaszi* were also present in the upper part of the column (Fig. 7, Electronic Supplement 5).

Besides foraminifera and ostracods, corallinacean and bryozoan (*Crisia* sp.) fragments are present in the upper part. Juvenile bivalve, small gastropods, and ooids are minor components.

Discussion

Sedimentology, mineralogy and geochemistry

The marls sampled along the investigated column show mineralogical and geochemical similarities and will therefore be discussed together. Due to their fine grain-size, the occurrence in the lower part of the column indicates deposition from suspension, while thin intercalations of coarser sediments represent periodic higher input of terrigenous material. During the Middle Miocene in the HZB, volcanism was not recorded (Šimunić et al. 1981, 1982; Aničić & Juriša 1984, 1985). The bentonite clay deposited within the horizontally-laminated marls probably indicates an airborne origin of distal tephra which landed in a marine environment, similarly to the bentonites deposited in the Badenian in Poljanska Luka (Gverić et al. 2020).

The upper part of the column consists of impure biocalcarenite, impure biocalcrudite, and fossiliferous litharenite within which marls are deposited. These coarse-grained sediments were likely deposited in high-energy environments by traction currents in a shallow-water environment (e.g., Vrsaljko et al. 2006). Petrographic composition and the occurrence of redeposited Badenian fossil fragments (Fig. 2) suggest strong terrigenous input and reworking of older sediments. However, intercalated marls indicate low-energy sedimentation. According to Vrsaljko et al. (2006), a similar depositional environment, but with a reduced salinity, existed during the Sarmatian as revealed by NCB strata documented at Medvednica Mt. in north Croatia. The described sedimentological characteristics and fossil content point to sedimentation in an inner-shelf environment.

Bentonite clay and marls

Variations in chemical composition of major elements are consistent with the mineralogy of the studied material; thus, marls and to a large extent bentonite clays both outline positive correlations of SiO_2, Na_2O, K_2O, and TiO_2 with alumina (Fig. 9).

Given their phyllosilicate budget, bentonite clays are solely made of montmorillonite (Fig. 3a). Its origin is related to the volcanic ash alteration in subaerial and submarine environments (Chamley 1989). Montmorillonite, as well as smectite in general, is transported much further than other minerals once in the ocean, since it becomes easily suspended in the form of colloidal particles (McKinley et al. 2003). Plagioclase was not unequivocally determined in XRD traces of bentonite clay and marls; however it was documented by SEM-EDS analysis (Fig. 3c). Significant amounts of opal-CT were documented in the studied bentonite, which we relate to the volcanic glass alteration as reported by Gverić et al. (2020) for the Badenian bentonites from the nearby Poljanska Luka. This furthermore may explain the lack of volcanic glass fragments in the bentonite investigated herein, bearing in mind that opal-CT, along with smectite and zeolite, is an omnipresent alteration product of volcanoclastic material (Christidis & Dunham 1997; Christidis 1998). In addition to smectite, opal-CT, and a high content of SiO_2 (60.69 %), a report on the presence of accessory minerals, such as euhedral zircon, apatite, biotite, and ilmenite corroborates the predominantly volcanic origin of the bentonite layer. In marls, except for detrital smectite,
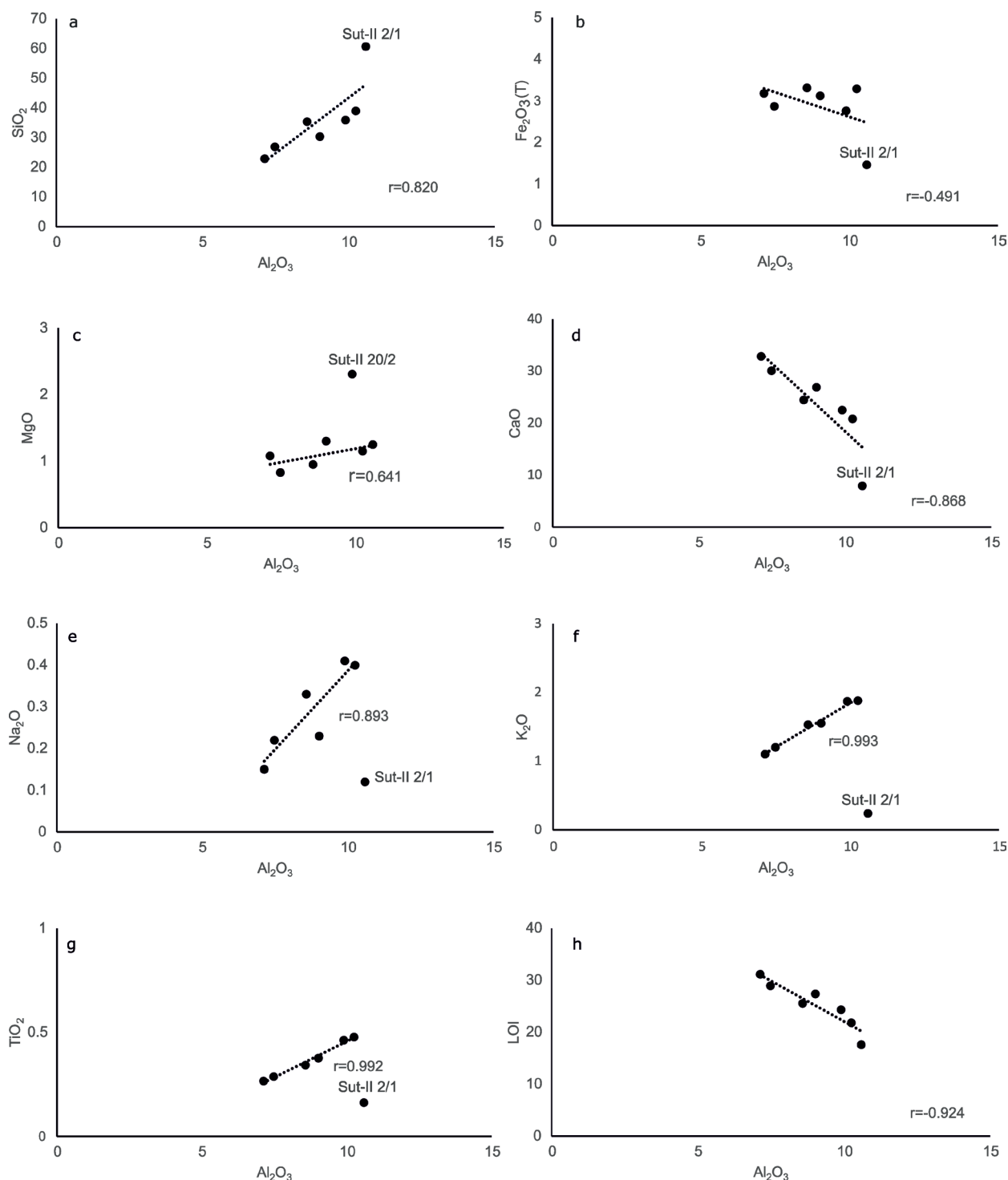
Fig. 9. Cross-plots of major oxides (wt. %) against Al_2O_3 (wt. %) showing the correlations.

there is an abundance of illite and kaolinite with traces of chlorite (Table 1). Illite and chlorite are typical terrigenous minerals formed directly from disintegrating parent rocks (Naidu et al. 1995; Lamy et al. 1998; Dianto et al. 2019). A small amount of chlorite in the analysed marls is attributed to its susceptibility to chemical weathering (Weaver 1989). However, a smaller amount of illite and chlorite might have

also come about through diagenetic processes, such as the illitization of smectite or alteration of K-feldspar, kaolinite, or biotite, respectively (Weaver 1989; Wilson 2004). Kaolinite, which does not intercalate with DMSO, is found predominantly in the studied marls (Table 1), which is in favour of the origin through the process of alteration and authigenesis. In contrast, kaolinite, which does intercalate with DMSO, is

presumably detrital and may be derived from kaolinite-bearing parent rocks (Durn 2003). In addition to clay minerals, a fraction of SiO_2 is attributed to quartz and, in the case of sample Sut-II 1/3, with cristobalite and bentonite clays with opal-CT (Table 1). There is a slightly weaker, positive correlation between MgO and Al_2O_3, from which the Sut-II 20/2 sample deviates because MgO is more related to the terrigenous input of dolomite than clay minerals. All samples show a good negative correlation of $Fe_2O_3(T)$, CaO and LOI with Al_2O_3 (Fig. 9b, d, h) because they are mostly related to the content of carbonates and not clay minerals. The bentonite clay sample again slightly deviates from this correlation. Apart from carbonates, $Fe_2O_3(T)$ is also associated with a small amount of ilmenite in bentonite clays and framboidal pyrite in some marl samples. The formation of calcite or aragonite in marls and bentonite clays is associated with biological and biochemical processes in the marine environment (Lippmann 1973; Rao 1996; Chang et al. 1998, Tišljar 2001). This accumulation is significantly reduced with a higher input of terrigenous siliciclastic material (Tišljar 2001), which is, in this case, volcanic ash.

A comparison of bentonite clay fractions shows that Sut-II 2/1 clay is systematically depleted in REE compared to Ugljevik-1 tuffaceous clay. Conversely, the normalisation curves' REE shapes tend to be similar between the two. The explanation for such discrepancy should be sought in the fact that Sutla-II bentonite contains a comparatively higher content of non-clay minerals with regards to Ugljevik-1 tuffaceous clay (Badurina & Šegvić 2022).

Provenance of sands, impure biocalcarenite, impure bio-calcrudite and fossiliferous litharenite

The mineral composition of the analysed sandy silt (Sut-II 11/1) and silty sand (Sut-II 19/1 and Sut-II 22/3) samples indicates a petrologically complex source area. Mineral associations consisted of undulose quartz, garnet, muscovite, chlorite, kyanite, and staurolite indicate predominantly metamorphic parent rocks (Mange & Maurer 1992). Mutić (1981) reports that garnet is the most common heavy mineral in the Miocene sandy sediments of the HZB. A low-grade metamorphic rocks provenance of the studied lithology is corroborated by the report of shist fragments in the LMF. A small amount of quartz with uniform extinction, zircon, and apatite could indicate the origin from igneous rocks (Mange & Maurer 1992). Tuffitic fragments in sands, impure biocalcarenite, impure biocalcrudite, and fossiliferous litharenite are undoubted indicators of pyroclastic source rocks (Fig. 4a). A part of the material is also derived from older sedimentary rocks, which is indicated by the presence of rounded zircon grains and dolomite, including glauconite in the impure biocalcarenite (Fig. 4). In general, impure biocalcarenite and biocalcrudite, as well as fossil litharenite, all contain numerous early Miocene and Badenian fossil fragments, individually-coated grains, and a significant amount of siliciclastic material, which suggests an intensive redeposition and a terrigenous input into the basin.

The general origin of the analysed Sarmatian clastic deposits is ambiguous. It is related to the various lithologies in the area of the uplifted blocks in the SW part of the PBS and the Inner Dinarides (Kovačić et al. 2011; Grizelj et al. 2017), including metamorphic, igneous, pyroclastic rocks, and older clastic sedimentary rocks. However, the position of the HZB suggests that the material input from locally uplifted blocks was more significant than from the Inner Dinarides compared to the NCB.

Biostratigraphy with regional events

Microfossils from the lower part of the column indicate the time of Badenian/Sarmatian transition. During that period, the sea level dropped in the entire Paratethys, which, together with tectonic movements, caused shallowing and restricted connections with an open sea (Krézsek & Filipescu 2005; Fordinál et al. 2006; Galović 2020). The abundant presence of *C. pataecus* (sample Sut-II 1/1; Fig. 6za, aa) indicates the proximity of the Badenian/Sarmatian boundary and defines the base and top of the Paratethyan Subzone PNN6d (12.8–12.18 Ma; Galović 2020, 2021). Mass occurrence of endemic species like *Anomalinoides dividens* (Krézsek & Filipescu 2005) within sample Sut-II 7/1 (Fig. 6a, b) points to the base of the regional transgression detected at 12.7 Ma, near the Badenian/Sarmatian boundary (Filipescu 2004; Krézsek & Filipescu 2005; Filipescu et al., 2014; Nováková et al. 2020; Peryt et al. 2021). This corresponds with *R. pseudoumbilicus* found in sample Sut-II 7/1 and supported by previous investigations within the other parts of NCB and HZB (Fig. 1b) (Galović 2020). This bioevent was documented from the Central to Eastern Paratethys (Chira & Mărunţeanu 2000) and can be regionally correlated. The Badenian–Sarmatian extinction event (BSEE=12.65 Ma) in the Carpathian foredeep approximates the Badenian/Sarmatian boundary (Palcu et al. 2015). In the Paratethys, the BSEE coincides with the subsequent sea level rise of the TB 2.6 cycle, dated at 12.64 Ma (Palcu et al. 2015), which correlates with the regional and global transgression (Van De Wal et al. 2011).

Based on the microfossil assemblage, the lower part of the investigated column is attributed to the foraminiferal *Anomalinoides dividens* Zone (Filipescu 2004), nannoplankton PNN6d (Galović 2020, 2021) and *Polysphaeridium zoharyi–Lingulodinium machaerophorum* Zone (Bakrač et al. 2012), characteristic for the Early Sarmatian.

The most numerous ostracod species in the upper part of the column are the stratigraphically important species *Cytheridea hungarica, Aurila merita*, and *Cytherois sarmatica* (Electronic Supplement 4) . The species *Cytheridea hungarica* and *Aurila mehesi* confirmed the Early Sarmatian age. Both species are zonal markers for the Early Sarmatian ostracod zone NO 11 *Cytheridea hungarica–Aurila mehesi* (Jiříček 1983; Jiříček & Říha 1991). The NO 11 zone is well correlated around the entire Central Paratethys and Lower Volhynian of the Eastern Paratethys (Jiříček & Říha 1991) and correlates with the *Anomalinoides dividens* and *Elphidium reginum* foraminiferal

zones (Grill 1941). The presence of *Elphidium reginum* (Fig. 6d) (sample Sut-II 19/1) attributes to the beginning of the *Elphidium reginum* Zone (Grill 1941) in the upper part of the investigated column.

Environmental interpretation

The lower part of the column points to unfavourable and fluctuating environmental conditions. The palaeosalinity indicators Sr/Ba (0.5 to 4.8, Electronic Supplement 2) imply marine environments (Wei & Algeo 2019). The lowest value is in sample Sut-II 7/1, indicating some freshwater influence, as confirmed by the palynofacies.

Reducing (anoxic-dysoxic) conditions are suggested by the redox proxies (Electronic Supplement 2), like the relatively low values of Th/U (0.98–1.81), except in the bentonite sample, and the values of the enrichment factors Mo_{EF} (2.36 to 9.94) and U_{EF} (6.67–10.15). A relatively higher value of Th/U (3.84) in the bentonite sample (Sut-II 2/1) could be related to its mineral composition. Only the uppermost sample (Sut-II 20/2) has a lower value of Mo_{EF} (2.05) and U_{EF} (2.30), pointing to a relatively higher oxygen content in bottom waters. This corresponds to the results of Tribovillard et al. (2012), where modest authigenic enrichment of Mo and U, with U_{EF}>Mo_{EF}, point to suboxic conditions. Data from Sutla-II are very similar to the data presented in Vlček et al. (2020). In the sediments of the Pozba–Vrable fms. of upper Badenian–Sarmatian age, Th/U varies between 1.4 and 4.3 (avg. 2.5) and Mo_{EF} from 0.7 to 10.3. A higher value of U_{EF} (6.67–10.15) in the lower part of Sutla-II could be connected to the carbonate content in the samples. Vlček et al. (2020) linked their results with the presence of a dysoxic event (Sarmatian dysoxic event).

Shallow and unfavourable conditions for ostracods are indicated based on their low diversity, broken valves, and present ontogenetic stages (mostly juvenile). A poorly-preserved foraminiferal assemblage composed of small-sized specimens also indicates a stressed environment and oxygen-deficient conditions. According to the palynofacies (high abundance of bisaccate pollen, where prasinophytes are more dominant in organic plankton) and nannoplankton (coccosphaeres) analyses, the lowest sample is deposited in a stable, stratified marine shelf with common *Holodiscolithus macroporus* (Perch-Nielsen 1985). Prasinophytes are considered a "disaster species", because they are most abundant when other phytoplankton taxa are absent and are found in sediments just above extinction horizons (Tappan 1980).

The presence of bolivinids in sample Sut-II 1/3 points to low oxic/anoxic conditions and low $CaCO_3$ content due to high input of organic material (Babejová-Kmecová et al. 2022 and references therein) at the sea bottom interrupted by short-time gateway(s) openings (Ruman 2017), which bring *Anomalinoides dividens* to the foraminiferal assemblage. Pseudo-planktonic life of *Anomalinoides dividens* can be observed in environments with a stratified water column, where oxygen deficiency suppresses most benthic life at the sea bottom, yet stimulates life in the upper, well-oxygenated layer (Filipescu 2004). According to Vrabac et al. (2015), the *Anomalinoides dividens* ecozone can be attributed to a low intertidal of a shallow subtidal zone. The malformed coccoliths and their low abundance in sample Sut-II 2/1 are most likely a consequence of acidification, which is also supported by the low carbonate concentration in the bentonite clay (Fig. 2).

The monospecific assemblage of *Anomalinoides dividens* (sample Sut- II 7/1) is also recorded in the Carpathian Foredeep Basin (Peryt et al. 2021) and interpreted as a bio-event that took place right after the BSEE and the interval with a depauperate foraminiferal assemblage composed of elphidiids and miliolids. According to the palynofacies (high share of phytoclasts and bisaccate pollen, dinocysts dominating among the organic plankton) and the dominance of *R. pseudoumbilicus* (Fig. 2), deposition took place on a proximal marine shelf, and shallower nearshore areas occasionally stratified under periodic terrigenous runoff (Tyson 1995; Galović 2017 and references therein). This occasionally-stratified, constantly-changing environment is also noted by the presence of framboidal pyrite and pyrite filling of foraminiferal chambers and palynomorphs as an indicator of low oxygen conditions associated with keeled elphidiids. Keeled elphidiids (epifaunal herbivorous species) are indicators of near normal marine conditions and relatively stable environments (Filipescu et al. 2014). Recent species of keeled elphidiids live in temperate to warm, shallow marine (depth up to 50 m) environments (inner shelf) (Szuromi-Korecz et al. 2021 and references therein). Numerous *Elphidium* species noted in a foraminiferal assemblage suggest environments enriched with iron (Žvab Rožič et al. 2022). Based on miliolids, the depositional environment points to the sea bottom overgrown by different seagrass or algae up to the depth of 60 m (Zlinská et al. 2010) and euryhaline conditions (based on *Anomalinoides dividens* and *Elphidium* spp.) according to Vlček et al. (2020). According to Babejová-Kmecová et al. (2022), a foraminiferal assemblage of dominant epiphytes (*Elphidium* spp., *Porosononion* spp.) and miliolids document strong short-term salinity fluctuation during sedimentation.

Due to the short-time opening of a gateway(s), the inner shelf environment was better oxygenated in the upper part of the column (samples from Sut-II 14/1 to Sut-II 20/2), resulting in better living conditions for the microfauna. Abundant and thick adult ostracods valves and carapaces, including burlier elphidiids and miliolids, indicate changed environmental conditions. Numerous, small, thin plant-dwellers species *Cytherois sarmatica*, as well as a few warmer water species of *Phlyctocythere pellucida* within sample Sut-II 14/1 may indicate a warmer, epi-neritic, plant-rich environment (Van Morkhoven 1963). *Phlyctocythere pellucida* is known from the Adriatic Sea (Uffenorde 1972). The shared finding of *C. sarmatica* and *P. pellucida* is known from Sarmatian deposits of the northern, marginal part of the Carpathian Foredeep (Szczechura 2000). Keeled epifaunal herbivorous (spinose *Elphidium reginum*, *Elphidium* spp.) and rounded infaunal

detritivorous specimens (*Nonion tumidulus, N. bogdanowiczi, Elphidiella serena*) indicate almost normal marine conditions and a highly stable environment (Filipescu et al. 2014). As chromatophore-bearing foraminifera, the keeled elphidiids must live in the euphotic zone under well-ventilated conditions (Szuromi-Korecz et al. 2021). The presence of *Borelis melo* (Fig. 6j), which are sizeable benthic foraminifera with photosynthetic diatom algal symbionts found in sample Sut-II 20/1, indicates minimum sea-surface temperatures greater than 18 °C and water depths of 5–65 m (Szuromi-Korecz et al. 2021 and references therein). A large number of reworked foraminifera and numerous redeposited Badenian ostracods in sample Sut-II 19/1 point to intense erosion of the basement. Fragments of partly uncoiled *Articulina* sp., together with cyprideids (*Miocyprideis, Hemicyprideis*), suggest shallow and less agitated water (Tóth & Görög 2008 and references therein).

In general, we can conclude that the early Sarmatian environment in which the investigated sediments were deposited, with the dominance of keeled elphidiids and miliolids among foraminifera and marine ostracod genera (*Aurila, Callistocythere, Loxoconha, Phyctenophora* and *Xestoleberis*), indicate a shallow water, calcium-carbonate rich environment (inner shelf) with significant changes in oxygen content due to fluctuations in freshwater inflow from the mainland (Babejová-Kmecová et al. 2022). A great abundance of epiphytic dweller foraminiferal taxa and phytal ostracods indicates an environment of the sea bottom covered by rich arborescent algal vegetation with water depths up to 50 m (Szuromi-Korecz et al. 2021) affected by the upcoming transgression.

Provenance and inferred regional geotectonic implications of bentonite clay and marls based on geochemical data

The diagram proposed by Winchester & Floyd (1977) shows that bentonite clay and its corresponding clay fraction both plot in the trachyandesite field (Fig. 10a), thereby suggesting an intermediate type of the source material.

The Ugljevik-1 clay fraction Nb/Y value is similar to that of the whole-rock Sut-II 2/1 bentonite (Fig. 10a). This posits Ugljevik-1 clay fraction in the field of alkali-basalts. The low Zr/TiO_2 values in the Ugljevik-1 clay fraction may represent an artefact of Ti residual enrichment, which is a common feature of entirely-altered bentonites (Hong et al. 2019). The same diagram was utilized in determining the origin of Badenian bentonites of the HZB (Poljanska Luka, Gverić et al., 2020), which indicates the felsic parent material. Furthermore, most Miocene bentonites and tuffs from the area of south-western PBS and the Dinaride Lake System analysed by Gverić et al. (2020) and Badurina et al. (2021) indicate parent material ranging from andesite through trachyandesite to rhyolite and trachyte respectively. According to the Ce/Yb–Ta/Yb discrimination diagram (Fig. 10b) (Pearce 1982), all samples reveal the shoshonite character, while Badurina et al. (2021) report a transitional, calc-alkaline to shoshonite characteristic of Miocene tuffs
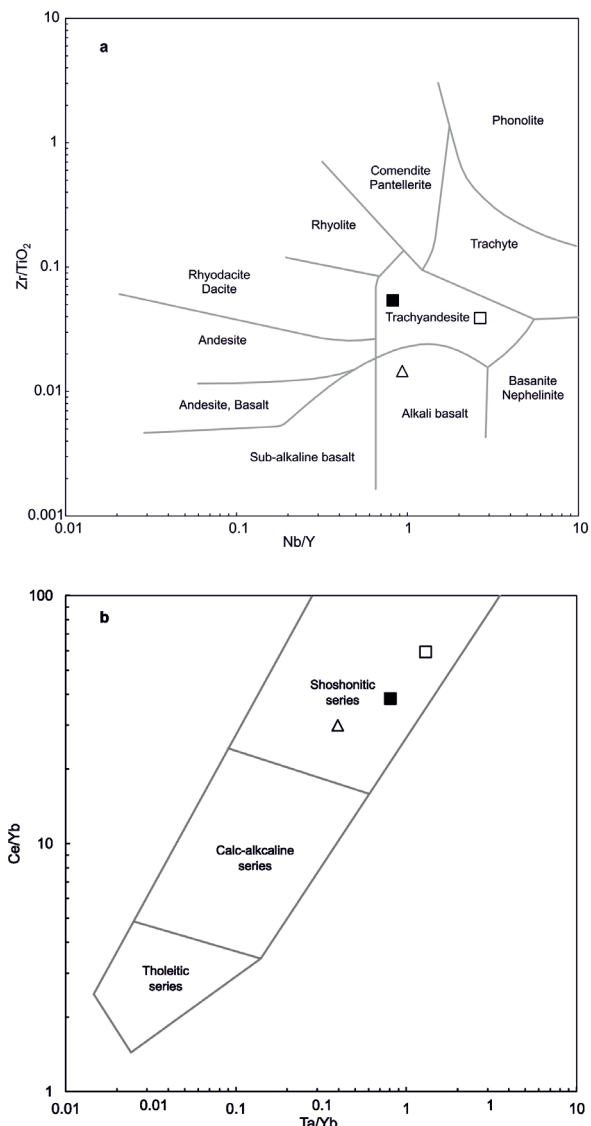

Fig. 10. a — Nb/Y vs. Zr/TiO_2 discrimination diagram (Winchester & Floyd 1977); **b** — Ce/Yb vs. Ta/Yb discrimination diagram (Pearce 1982) for the analysed samples. Black square – bentonite, empty square – Sut-II 2/1 CF, triangle – Ugljevik-1 CF.

from Alpine lakes scattered throughout the nearby Dinaridic orogen.

The La–Th–Sc diagram used to determine provenance of sedimentary rocks (Cullers 1994) indicates that the marls originated from rocks of a mixed source (Fig. 11a).

Since bentonite clays represent altered volcanic ash transported by wind or air currents into the sedimentation basin and may therefore contain some intra-basin and terrigenous material, the same diagram was used for bentonite clays, indicating a source from felsic rocks. The chemical composition of all samples and elemental ratios susceptible to provenance, such as Eu/Eu*, La/Sc, Th/Sc, La/Co, Th/Co, LREE/HREE (Electronic Supplement 2), correspond to the values for felsic rocks (Cullers 1994; 2000). We can conclude that all marly samples were likely formed by weathering of different
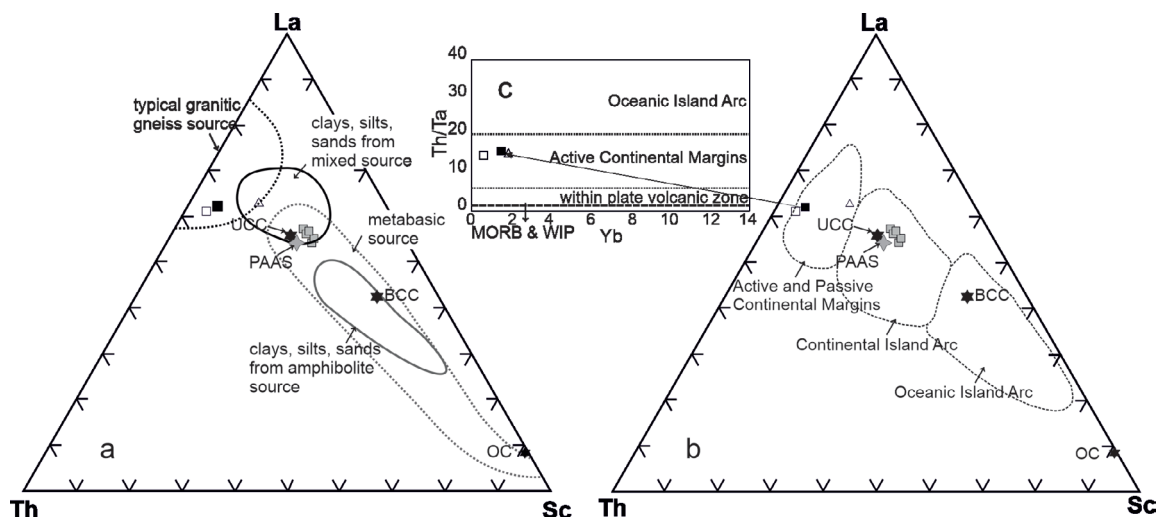
Fig. 11. Ternary plots La–Th–Sc: **a** — for provenance analyses (Cullers 1994), **b** — for tectonic settings (Bhatia & Crook 1986), **c** — discrimination Th/Ta vs. Yb for tectonic settings (Gorton & Schandl 2000). Average composition of Upper Continental Crust (UCC), Post-Archean Australian Shale (PAAS), Bulk Continental Crust (BCC) and Ocean Crust (OC) after Taylor & McLennan (1985) are additionally plotted. Black square – bentonite, grey square – marls, empty square – Sut-II 2/1 CF, triangle – Ugljevik-1 CF.

(mixed) types of (volcanic, metamorphic, older sedimentary) rocks and are mostly felsic in nature, similarly to the coarse-grained samples from the upper part of the column as evidence by mineralogical results. However, elemental ratios proposed by Cullers (1994, 2000) distinguish only extremely felsic or mafic source rocks, but not the intermediate ones. The possible reason for discrepancies shown by these discriminant diagrams for the bentonite clay may be due to the manner of their formation. Namely, these bentonite clays were formed by weathering of the material that could have been affected by winnowing during long-distance transport (Gverić et al. 2020). Additionally, Christidis (1998) demonstrates that the variable mobility of Y, which is accompanied by residual enrichment of Zr and Nb in altered felsic rocks, make the diagram of Winchester & Floyd (1977) of limited value when assessing the alkaline character of altered felsic rocks. Furthermore, recent work by Namayandeh et al. (2020) suggests that Ti, Gd, Ga, Pr, Tb, Nd, Sm, Ce, and Nb are comparatively immobile, while elements, such as U, Dy, In, Sc, Hf, Zr, La, and Eu are poorly mobile during the alteration of volcanic ash in a marine setting. These suggest that discrimination diagrams relying on the elemental concentrations mentioned above should be interpreted with caution when dealing with altered felsic rocks.

To determine tectonic settings of marls, the La–Th–Sc diagram proposed by Bhatia & Crook (1986) was used (Fig. 11b). All marls plot close to the average composition of the Upper Continental Crust (UCC) (Taylor & McLennan 1985), as well as within the field of the Continental Island Arc (Fig. 11b) which, according to Bhatia & Crook (1986), comprises an inter-arc or fore-arc, or back-arc basin, developed along a volcanic-arc on a thick continental crust or thin continental margins. Furthermore, the whole-rock and clay fraction of bentonite clay and Ugljevik-1 are displayed in the common field of Active and Passive Continental Margin in this

diagram, as well as the Active Continental Margin (ACM) in the geotectonic provenance discrimination diagram Th/Ta–Yb/Ta according to Gorton & Schandl (2000) (Fig. 11c), which would be consistent with their volcanic origin. Reworked Miocene tuffs and rare dome-flow complexes are widespread along the whole CPR (Pécskay et al. 1995, 2006; Lexa et al. 2010). All marls show significant negative Nb–Ta anomalies (Fig. 10c), while bentonite clay with analysed clay fractions show the highest Nb values. This negative anomaly in bentonite clay is likely masked by the more pronounced K anomaly. The negative anomalies of Ti and a Nb–Ta pair are typical for subduction-related magmas (e.g., Slovenec & Šegvić 2021), which is consistent with the evolution of CPR in the Middle Miocene (Royden 1988; Konečný et al. 2002; Lexa et al. 2010).

Badenian bentonite clays of Poljanska Luka deposit are located on the opposite wing of the anticline compared to the location of the Sutla-II column (Aničić & Juriša 1984) (Fig. 1b). The geological sequence of Poljanska Luka consists of marls and bioclastic limestones with two layers of bentonite within two different horizons of altered tuffites (Braun 1991). The smectites within the bentonite clays there were classified as beidellitic montmorillonite (Gverić et al. 2020).

According to Braun (1991) and Gverić et al. (2020), the time of deposition of the Poljanska Luka tuffs (Badenian) in conjunction with the Sut-II 2/1 tuffs (Early Sarmatian) in this study, corresponds to the time when tuffs in the area of Ugljevik (~14.2 and 12.5 Ma) were deposited (Mandic et al. 2019). Badurina et al. (2021) suggest that the Upper Middle Miocene tuffaceous clay from the Ugljevik area is associated with calc-alkaline magmatism of the eastern segment of the CPR, especially the Apuseni Mts. and/or Eastern Carpathians. This was confirmed by the similarity of the chemical composition of trace elements between the Lower Sarmatian

tuffaceous clay from Ugljevik-1 with magmatic rocks from the Apuseni Mts. (Badurina et al. 2021). Low values of Nb and Zr (Nb 5–12 ppm, Zr 50–150 ppm) from the Apuseni Mts. (Rosu et al. 2004) correlate well with the Nb and Zr values from tuffaceous clay from Ugljevik about 340 km away (Nb 3.9–16.1 ppm, Zr 50.7–202, 2 ppm) (Badurina et al. 2021) and bentonite clays from this study (Nb 10.5 ppm; Zr 88 ppm) 550 km away. Additionally, a direct comparison of clay fractions of Sut-II 2/1 and Ugljevik-1 further corroborated their shared geochemical affinity. This is clearly outlined by the comportment of immobile trace elements such as Nb, Ta, Th and U (Fig. 9c, d) and placements in multiple geotectonic diagrams (Fig. 10, 11).

There is, however, a paucity of evidence in favour of Lower Sarmatian volcanism of the northern and eastern parts of the Carpathian–Pannonian region and Apuseni Mts., which was potent enough to give rise to distal tephra that could have potentially reached the study area. On the other hand, during the Badenian to Early Pannonian period (14.5–9.5 Ma), extensive felsic to intermediate volcanic activity took place in the area of the Tokay–Zemplín–Beregovo–Oaş Mts. (Péckay et al. 2006; Lexa et al. 2010). Based on the comparable age (11.5±0.5 Ma) and geochemical composition, Danšík et al. (2021) pointed to this volcanism as parental to the 1500 km-distant Gorelka tephra in SW Russia. The material was transported by westerly winds, which were typical of the atmospheric circulation regime in Central Europe during the Tortonian age. Conversely, during the Serravallian (late Middle Miocene, 13.82–11.62 Ma), Europe was likely dominated by trade winds blowing from the NNE to the SSW (Quan et al. 2014; Šegvic et al. 2022), thus indicating the eastern source of volcanic material deposited in the investigated area.

Conclusions

Biostratigraphically, the analysed deposits belong to the Early Sarmatian. The lower part of the investigated column is attributed to the foraminiferal *Anomalinoides dividens* Zone, nannoplankton subzone PNN6d, and dinocyst *Polysphaeridium zoharyi–Lingulodinium machaerophorum* Zone. The upper part of the column indicates the onset of foraminiferal *Elphidium reginum* Zone and ostracod Zone NO 11.

The deposition of volcanic ash recognised within the Sutla-II column took place in the Early Sarmatian marine, inner shelf environment. The layer of bentonite clay is predominantly composed of montmorillonite and opal-CT formed by the alteration of volcanic ash. The volcanic ash stems from felsic to intermediate volcanism and was deposited between horizontally-laminated marls. The described occurrence of bentonite clay at the Sutla-II column is associated with a distant volcanic eruption. The time of deposition and similarity of the trace elements composition of the Lower Sarmatian bentonite clay from Sutla-II and tuffaceous clay from Ugljevik-1 suggest a possible connection with the same eruption of the volcanoes in the north-eastern part of the CPR.

Provenance analysis based on trace elements showed that marls were sourced from a composite, predominantly felsic source. Terrigenous smectite, and to a lesser degree diagenetic smectite, which procured through tuff alteration, is the most abundant clay mineral in the studied marls. Deposition of the lower part of the column took place on a proximal marine shelf, and shallower nearshore areas occasionally stratified under periodic terrigenous runoff, while deposition of the upper part took place in a shallow, inner shelf, high-energy environment, consisting of impure biocalcarenite, impure biocalcrudite, fossiliferous litharenite characterised by intensive redeposition of older rocks and fossils. Provenance analyses based on heavy minerals on sandy samples also indicate the origin from mixed sources, among which metamorphic rocks predominate.

References

Algeo T.J. & Li C. 2020: Redox classification and calibration of redox thresholds in sedimentary systems. *Geochimica et Cosmochimica Acta* 287, 8–26. https://doi.org/10.1016/j.gca.2020.01.055

Aničić B. & Juriša M. 1984: Basic Geological Map of SFRY 1:100000, Rogatec sheet L33-68 Geološki zavod, Ljubljana, *Geološki zavod Zagreb*, *Savezni geološki zavod*, Beograd (in Slovenian).

Aničić B. & Juriša M. 1985: Basic Geological Map of SFRY 1:100000, Geology of the Rogatec sheet L33-68. *Geološki zavod Ljubljana in Geološki zavod Zagreb*, *Savezni geološki zavod*, Beograd, 1–76 (in Slovenian).

Avanić R. 2012: Lower Miocene lithostratigraphic units from northwestern Croatia. *PhD Thesis*, *Faculty of Science, University of Zagreb*, 1–162 (in Croatian with English Summary).

Avanić R., Šimunić An., Hećimović I., Kovačić Ma., Marković S., Grgasović T., Kurečić T., Slovenec D. & Vrsaljko D. 2015: Basic Geological Map of RH 1:50000. Geology of the Trakošćan (Ptuj 2) sheet. *Hrvatski geološki institut, Zavod za Geologiju*, Zagreb (in Croatian).

Avanić R., Kovačić M., Pavelić D. & Peh Z. 2018: The Neogene of Hrvatska Zagorje. In: Tibljaš D., Horvat M., Tomašić N., Mileusnić M. & Grizelj A. (Eds.): 9th Mid-European Clay Conference. *Conference book, Field Trip Guide book*, Zagreb, 128–129.

Avanić R., Pavelić D., Pécsay Z., Miknić M., Tibljaš D. & Wacha L. 2021: Tidal deposits in the Early Miocene Central Paratethys: The Vučji Jarek and Čemernica members of the Macelj formation (NW Croatia). *Geologia Croatica* 74, 41–56. https://doi.org/10.4154/gc.2021.06

Babejová-Kmecová J., Plašienková I., Sliva Ľ., Halásová E. & Hudáčková N. 2022: From dysoxic sea to hypersaline lagoon: paleoenvironmental changes on the Badenian/Sarmatian boundary (borehole MZ 102; Vienna Basin). *Acta Geologica Slovaca* 14, 57–72.

Badurina L. & Šegvić B. 2022: Assessing trace-element mobility during alteration of rhyolite tephra from the Dinaride Lake System using glass-phase and clay-separate laser ablation inductively coupled plasma mass spectrometry. *Clay Minerals* 57, 1–6. https://doi.org/10.1180/clm.2022.12

Badurina L., Šegvić B., Mandic O. & Slovenec D. 2021: Miocene tuffs from the Dinarides and Eastern Alps as proxies of the Pannonian Basin lithosphere dynamics and tropospheric circulation patterns in Central Europe. *Journal of the Geological Society* 178, 2020–2062. https://doi.org/10.1144/jgs2020-262

Bakrač K., Koch G., Sremac J. 2012: Middle and Late Miocene palynological biozonation of the south-western part of Central Paratethys (Croatia). *Geologia Croatica* 65, 207–222. https://doi.org/10.4154/GC.2012.12

Behr Labor-Technik 2017: SCM1 Calcimeter for determination of the carbonate content of a soil sample. *User's Manual*, 1–15.

Bhatia M.R. & Crook K.A.W. 1986: Trace Element Characteristics of Greywackes and Tectonic Setting Discrimination of Sedimentary Basins. *Contributions to Mineralogy and Petrology* 92, 181–193. https://doi.org/10.1007/BF00375292

Biscaye P.E. 1965: Mineralogy and Sedimentation of Recent Deep-Sea Clay in the Atlantic Ocean and Adjacent Seas and Oceans. *GSA Bulletin* 76, 803–832. https://doi.org/10.1130/0016-7606 (1965)76[803:MASORD]2.0.CO;2

Braun K. 1991: Mineralogical-petrographical characteristics and genesis of the bentonite deposits of Maovice, Gornja Jelenska, Bednja and Poljanska Luka. *Acta Geologica* 21, 1–34 (in Croatian with English Abstract).

Brlek M., Iveša L., Brčić V., Santos A., Ćorić S., Milošević M., Avanić R., Devescovi M., Pezelj Đ., Mišur I. & Miknić M. 2018: Rocky-shore unconformities marking the base of Badenian (Middle Miocene) transgressions on Mt. Medvednica basement (North Croatian Basin, Central Paratethys). *Facies* 64, 1–25. https://doi.org/10.1007/s10347-018-0537-0

Brlek M., Kutterolf S., Gaynor S., Kuiper K., Belak M., Brčić V., Holcová K., Wang K., Bakrač K., Hajek-Tadesse V., Mišur I., Horvat M., Šuica S. & Schaltegger U. 2020: Miocene syn-rift evolution of the North Croatian Basin (Carpathian–Pannonian Region): new constraints from Mts. Kalnik and Požeška gora volcaniclastic record with regional implications. *International Journal of Earth Science* 109, 2775–2800. https://doi.org/10.1007/s00531-020-01927-4

Chamley H. 1989: Clay sedimentology. *Springer Verlag*, Berlin, 1–623.

Chang L.L.Y., Howie R.A. & Zussman M.A. 1998: Rock forming minerals, Vol. 5B, Non-silicates: Sulphates, Carbonates, Phosphates, Halides. *Geological Society of London*, London, 1–383.

Chira C.M. & Mărunțeanu M. 2000: Calcareous nannofossils and dinoflagellates from the Middle Miocene of the Transylvanian basin, Romania. INA 8 Bremen abstracts. *Journal of Nannoplankton Research* 22, 89–90.

Christidis G.E. 1998: Comparative study of the mobility of major and trace elements during alteration of an andesite and a rhyolite to bentonite, in the islands of Milos and Kimolos, Aegean, Greece. *Clays and Clay minerals* 46, 379–399. https://doi.org/10.1346/CCMN.1998.0460403

Christidis G. & Dunham A. C. 1997: Compositional variations in smectites: Part II. Alteration of acidic precursors. A case study from Milos Island. Greece. *Clay Minerals* 32, 253–270. https://doi.org/10.1180/claymin.1997.032.2.07

Ćorić S., Pavelić D., Rögl F., Mandic O., Vrabac S., Avanić R., Jerković L. & Vranjković A. 2009: Revised Middle Miocene datum for initial marine flooding of North Croatian Basins (Pannonian Basin System, Central Paratethys). *Geologia Croatica* 62, 31–43. https://doi.org/10.4154/GC.2009.03

Csontos L., Márton E., Wórum G. & Benkovics L. 2002: Geodynamics of the SW-Pannonian inselbergs (Mecsek and Villány Mts., SW Hungary): Inferences from a complex structural analysis. In: Cloetingh S.A.P.L., Horváth F., Bada G. & Lankreijer A.C. (Eds.): Neotectonics and surface processes: the Pannonian Basin and Alpine/Carpathian System. *Stephan Mueller Spec. Publ.* 3, 227–246.

Cullers R.L. 1994: The chemical signature of source rocks in size fractions of Holocene stream sediment derived from metamorphic rocks in the Wet Mountains region, Colorado U.S.A. *Chemical Geology* 113, 327–343.

Cullers R.L. 2000: The geochemistry of shales, siltstones and sandstones of Pennsylvanian-Permian age, Colorado, USA: Implications for provenance and metamorphic studies. *Lithos* 51, 181–203.

Dianto A., Subehi L., Ridwansyah I. & Hantoro W.S. 2019: Clay minerals in the sediments as useful paleoclimate proxy: Lake Sentarum case study, West Kalimantan, Indonesia. *IOP Conference Series: Earth and Environmental Science* 311, 012036. https://doi.org/10.1088/1755-1315/311/1/012036

Durn G. 2003: Terra Rossa in the Mediterranean Region: Parent Materials, Composition and Origin. *Geologia Croatica* 56, 83–100. https://doi.org/10.4154/GC.2003.06

Filipescu S. 2004: *Anomalinoides dividens* bioevent at the Badenian/Sarmatian boundary – a response to paleogeographic and paleoenvironmental changes. *Studia Universitatis Babeș-Bolyai, Geologia* 49, 21–26. https://doi.org/10.5038/1937-8602.49.2.3

Filipescu S., Miclea A., Gross M., Harzhauser M., Zágoršek K., & Jipa C. 2014: Early Sarmatian paleoenvironments in the easternmost Pannonian basin (Borod depression, Romania) revealed by the micropaleontological data. *Geologica Carpathica* 65, 67–81. https://doi.org/10.2478/geoca-2014-0005

Fodor L., Csontos L., Bada G., Győrfi I. & Benkovics L. 1999: Tertiary tectonic evolution of the Pannonian basin system and neighbouring orogens: a new synthesis of palaeostress data. In: Durand B., Jolivet L., Horváth F. & Séranne M. (Eds.): The Mediterranean Basins: Tertiary extension within the Alpine Orogene. *Blackwell Sciences Special Publications of the Geological Society of London*, Oxford, 295–334

Fordinál K., Zágoršek K. & Zlinská A. 2006: Early Sarmatian biota in the northern part of the Danube Basin (Slovakia). *Geologica Carpathica* 57, 123–130.

Galović I. 2017: Sarmatian calcareous nannofossil assemblages in the SW Paratethyan marginal marine environments: implications for palaeoceanography and the palaeoclimate. *Progress in oceanography* 156, 209–220. https://doi.org/10.1016/j.pocean.2017.05.011

Galović I. 2020: Sarmatian biostratigraphy of a marginal sea in northern Croatia based on calcareous nannofossils. *Marine Micropaleontology* 161. https://doi.org/10.1016/j.marmicro.2020.101928

Galović I. 2021: Corrigendum to «Sarmatian biostratigraphy of a marginal sea in northern Croatia based on calcareous nannofossils» [Marine Micropaleontology 101928 161 (2020)]. *Marine Micropaleontology* 167. https://doi.org/10.1016/j.marmicro.2021.102011

Galović I. & Bajraktarević Z. 2006: Sarmatian biostratigraphy of the Mt. Medvednica at Zagreb based on siliceous microfossils (North Croatia, Central Paratethys). *Geologica Carpathica* 57, 199–210.

Gorton M.P. & Schandl E.S. 2000: From continents to island arcs: a geochemical index of tectonic setting for arc-related and within-plate felsic to intermediate volcanic rocks. *Canadian Mineralogist* 38, 1065–1073. https://doi.org/10.2113/gscanmin.38.5.1065

Greene-Kelly R. 1953: Irreversible dehydration in montmorillonite, Part II. *Clay Mineral Bulletin* 1, 52–56.

Greene-Kelly R. 1955: Dehydration of montmorillonite minerals. *Mineralogical Magazine* 30, 604–615.

Grill R. 1941: Stratigraphische Untersuchungen mit Hilfe von Mikrofaunen im Wiener Becken und den benachbarten Molasse-Anteilen. *Öl Kohle* 37, 595–602.

Grizelj A., Peh Z., Tibljaš D., Kovačić M. & Kurečić T. 2017: Mineralogical and geochemical characteristics of Miocene pelitic sedimentary rocks from the south-western part of the Pannonian Basin System (Croatia): Implications for provenance studies. *Geoscience Frontiers* 8, 65–80. https://doi.org/10.1016/j.gsf.2015.11.009

Grizelj A., Milošević M., Bakrač K., Galović I., Kurečić T., Hajek-Tadesse V., Avanić R., Miknić M., Horvat H., Čaić Janković A. & Matošević M. 2020: Palaeoecological and sedimentological characterisation of Middle Miocene sediments from the Hrvatska Kostajnica area (Croatia), *Geologia Croatica* 73, 153–175. https://doi.org/10.4154/gc.2020.15

Gverić Z., Hanžel D., Kampić Š., Pleša A. & Tibljaš D. 2020: Comprehensive characterisation of bentonites from Croatia and neighbouring countries. *Geologia Croatica* 73. 29–48. https://doi.org/10.4154/gc.2020.02

Handy M.R., Ustaszewski K. &, Kissling E. 2015: Reconstructing the Alps–Carpathians–Dinarides as a key to understanding switches in subduction polarity, slab gaps and surface motion. *International Journal of Earth Sciences* 104, 1–26. https://doi.org/10.1007/s00531-014-1060-3

Harangi S. & Lenkey L. 2007: Genesis of the Neogene to Quaternary volcanism in the Carpathian-Pannonian region: Role of subduction, extension, and mantle plume. *Special Papers – Geological Society of America* 418, 67–67, https://doi.org/10.1130/2007.2418(04)

Harzhauser M. & Piller W.E. 2007: Benchmark data of a changing sea – Palaeogeography, palaeobiogeography and events in the Central Paratethys during the Miocene. *Palaeogeography, Palaeoclimatology, Palaeoecology* 253, 8–31. https://doi.org/10.1016/j.palaeo.2007.03.031

Hong H., Algeo T.J., Fang Q., Zhao L., Ji K., Yin K., Wang C. & Cheng S. 2019: Facies dependence of the mineralogy and geochemistry of altered volcanic ash beds: An example from Permian–Triassic transition strata in southwestern China. *Earth-Science Reviews* 190, 58–88. https://doi.org/10.1016/j.earscirev.2018.12.007

Hrvatski Geološki Institut 2009: Geological Map of the Republic of Croatia scale 1:300.000. *Hrvatski geološki institut (Croatian Geological Survey)*, Zagreb, 1 sheet.

International Centre for Diffraction Data 2021: PDF-4/Minerals, SN: MIND 210134-1834.

Jackson M.L. 1956: Soil chemical analysis – Advanced course. Medison. Wisconsin, published by the author, 1–984. https://doi.org/10.1002/jpln.19590850311

Jiříček R. 1983: Redefinition of the Oligocene and Neogene Ostracod Zonation of the Paratethys. Miscellanea Micropaleontology. A memorial volume dedicated to the 18th European Colloquium on Micropaleontology, 195–236.

Jiříček R. & Říha J. 1991: Correlation of Ostracod Zones in the Paratethys and Tethys. *Saito Ho–on Kai Special Publications* (Proceedings of Shallow Tethys) 3, 435–457.

Kiss P., Gméling K., Molnár F. & Pécskay Z. 2010: Geochemistry of Sarmatian volcanic rocks in the Tokaj Mts (NE Hungary) and

their relationship to hydrothermal mineralization. *Central European Geology* 53, 377–403. https://doi.org/10.1556/CEuGeol.53.2010.4.3

Konečný V., Kováč M., Lexa L. & Šefara J. 2002: Neogene evolution of the Carpatho-Pannonian region: an interplay of subduction and back-arc diapiric uprise in the mantle. *EGU Stephan Mueller Special Publication Series* 1, 105–123. https://doi.org/10.5194/smsps-1-105-2002

Kopecká J., Holcová K., Brlek, M., Scheiner F., Ackerman L., Rejšek J., Milovský R., Baranyi V., Gaynor S., Galović I., Brčić V., Belak M. & Bakrač K. 2022: A case study of paleoenvironmental interactions during the Miocene Climate Optimum in southwestern Paratethys. *Global and Planetary Change* 211. https://doi.org/10.1016/j.gloplacha.2022.103784

Kováč M., Hudáčková N., Halásová E., Kováčová M., Holcová K., Oszczypko-Clowes M., Báldi K., Less G., Nagymarosy A., Ruman A., Klučiar T. & Jamrich M. 2017: The Central Paratethys palaeoceanography: A water circulation model based on microfossil proxies, climate, and changes of depositional environment. *Acta Geologica Slovaca* 9, 75–114.

Kováč M., Halásová E., Hudáčková N., Holcová K., Hyžný M., Jamrich M. & Ruman A. 2018: Towards better correlation of the Central Paratethys regional time scale with the standard geological time scale of the Miocene Epoch. *Geologica Carpathica* 69, 283–300. https://doi.org/10.1515/geoca-2018-0017

Kovačić M., Horvat M., Pikija M. & Slovenec D. 2011: Composition and provenance of Neogene sedimentary rocks of Dilj gora Mt. (south Pannonian Basin, Croatia). *Geologia Croatica* 64, 121–132.

Kovačić M., Marković F., Ćorić S., Pezelj Đ., Vrsaljko D., Bakrač K., Hajek-Tadesse V., Ritossa A. & Tarnaj I. 2015a: Disintegration of the Central Paratethys and origin of the Lake Pannon. In: Kovačić M., Wacha L. & Horvat M. (Eds.): 7th International workshop on the Neogene from the Central and South-eastern Europe. Field trip guide book. Zagreb, 22–25.

Kovačić M., Vrsaljko D., Pezelj Đ., Premec Fućek V., Hernitz Kučenjak M., Galović I., Ćorić S., Zalović M. & Marković F. 2015b: A Middle Miocene marine deposition with pyroclastics. In: Kovačić M., Wacha L. & Horvat M. (Eds.): 7th International workshop on the Neogene from the Central and South-eastern Europe. Field trip guide book Zagreb, 19–21.

Kovacs M., Pécskay Z., Fülöp A., Jurje M. & Edelstein O. 2013: Geochronology of the Neogene intrusive magmatism of the Oas–Gutâi Mountains, Eastern Carpathians (NW Romania). *Geologica Carpathica* 64, 483–496. https://doi.org/10.2478/geoca-2013-0033

Krézsek C. & Filipescu S. 2005: Middle to late Miocene sequence stratigraphy of the Transylvanian Basin (Romania). *Tectonophysics* 410, 437–463. https://doi.org/10.1016/j.tecto.2005.02.018

Krumm S. 1994: Centrifuge, Erlangen. http://www.ccp14.ac.uk/ccp/web-mirrors/krumm/html/software/winsoft.html.

Lamy F., Hebbeln D. & Wefer G. 1998: Terrigenous sediment supply along the Chilean continental margin: modern regional patterns of texture and composition. *Geologische Rundschau* 87, 477–494. https://doi.org/10.1007/s005310050223

Lexa J., Seghedi I., Németh K., Szakács A., Konečný V., Pécskay Z., Fülöp A.& Kovacs M. 2010: Neogene-Quaternary Volcanic forms in the Carpathian-Pannonian Region: a review. Central European. *Journal of Geosciences* 2, 207–270. https://doi.org/10.2478/v10085-010-0024-5

Lippmann F. 1973: Sedimentary carbonate minerals. *Springer Verlag*, Berlin, 1–228.

Mandic O., De Leeuw A., Bulić J., Kuiper K.F., Krijgsman W. & Jurišić-Polšak Z. 2012: Paleogeographic evolution of the southern Pannonian Basin: 40Ar/39Ar age constraints on the Miocene continental series of northern Croatia. *International*

Journal of Earth Science 101, 1033–1046. https://doi.org/10.1007/s00531-011-0695-6

Mandic O., Sant K., Kallanxhi M.E., Ćorić S., Theobalt D., Grunert P., De Leeuw A. & Krijgsman W. 2019: Integrated bio-magneto-stratigraphy of the Badenian reference section Ugljevik in southern Pannonian Basin - implications for the Paratethys history (middle Miocene, Central Europe). *Global and Planetary Changes* 172, 374–395. https://doi.org/10.1016/j.gloplacha.2018.10.010

Mange M.A. & Maurer H.F.W. 1992: Heavy Minerals in Colour. *Chapman and Hall*, London, 1–142.

Marković F. 2017: Miocene tuffs from North Croatian Basin. *PhD Thesis*, *Faculty of Science, University of Zagreb*, 1–174 (in Croatian with English Abstract).

Marković F., Kuiper K., Ćorić S., Hajek-Tadesse V., Hernitz Kučenjak M., Bakrač K., Pezelj Đ. & Kovačić M. 2021: Middle Miocene marine flooding: new $^{40}Ar/^{39}Ar$ age constraints with integrated biostratigraphy on tuffs from the North Croatian Basin. *Geologia Croatica* 74, 237–252. https://doi.org/10.4154/gc.2021.18

Marković S. 2002: Croatian mineral resources (in Croatian). *Institute of geology*, Zagreb, 1–543.

McKinley J.M., Worden R.H. & Ruffell A.H. 2003: Smectite in Sandstones: A Review of the Controls on Occurrence and Behaviour During Diagenesis. *International Association of Sedimentologists Special Publication* 34, 109–128. https://doi.org/10.1002/9781444304336.ch5

Moore D.M. & Reynolds R.C. Jr. 1997: X-ray diffraction and the identification and analysis of clay Minerals. *Oxford University Press*, Oxford, 1–378.

Moore P.D., Webb J.A. & Collinson M. 1991: Pollen Analysis (second edition). *Blackwell Sci. Publication*, London, 1–216.

Mutić R. 1981: Heavy minerals occurring in Miocene beds of Hrvatsko zagorje – North-western part. *Geološki vjesnik* 33, 145–167.

Nagy N.M. & Kónya J. 2005: The relations between the origin and some basic physical and chemical properties of bentonite rocks illustrating on the example of Sarmatian bentonite site at Sajóbábony (HU). *Applied Clay Science* 28, 257–267. https://doi.org/10.1016/j.clay.2004.02.007

Naidu A.S., Han M.W., Mowatt T.C. & Wajda W. 1995: Clay minerals as indicators of sources of terrigenous sediments, their transportation and deposition: Bering Basin, Russian-Alaskan Arctic. *Marine Geology* 127, 87–104. https://doi.org/10.1016/0025-3227(95)00053-2

Namayandeh A., Modabberi S. & López-Galindo A. 2020: Trace and rare earth Element distribution and mobility during diagenetic alteration of volcanic ash to bentonite in eastern Iranian bentonite deposits. *Clays and Clay Minerals* 68, 50–66. https://doi.org/10.1007/s42860-019-00054-9

Nováková P., Rybár S., Šarinová K., Nagy A., Hudáčková N., Jamrich, M., Teodoridis V., Kováčová M., Šujan M., Vlček T. & Kováč M. 2020: The late Badenian-Sarmatian (Serravallian) environmental transition calibrated by sequence stratigraphy (eastern Danube Basin, Central Paratethys). *Geologica Carpathica* 71, 291–313. https://doi.org/10.31577/GeolCarp.71.4.1

Palcu D.V., Tulbure M., Bartol M., Kouwenhoven T.J. & Krijgsman W. 2015: The Badenian-Sarmatian Extinction Event in the Carpathian foredeep basin of Romania: Paleogeographic changes in the Paratethys domain. *Global and Planetary Change* 133, 346–358. https://doi.org/10.1016/j.gloplacha.2015.08.014.

Pamić J. 1997: Volcanic rocks from the Sava-Drava interfluve and Baranja in the south Pannonian basin (Croatia). *Nafta*, Zagreb, 1–192 (in Croatian).

Pamić J. & Pécskay Z. 1996: Geochronological and K/Ar ages of Tertiary volcanic formations from the southern part of the Pannonian Basin in Croatia – based on surface and subsurface data. *Nafta* 47, 195–202.

Pavelić D. 2001: Tectonostratigraphic model for the North Croatian and North Bosnian sector of the Miocene Pannonian Basin System. *Basin Research* 13, 359–376. https://doi.org/10.1046/j.0950-091x.2001.00155.x

Pavelić D. & Kovačić M. 2018: Sedimentology and stratigraphy of the Neogene rift-type North Croatian Basin (Pannonian Basin System, Croatia): A review. *Marine and Petroleum Geology* 91, 455–469. https://doi.org/10.1016/j.marpetgeo.2018.01.026

Pavelić D., Avanić R., Kovačić M., Vrsaljko D. & Miknić M. 2003: An Outline of the Evolution of the Croatian Part of the Pannonian Basin System. In: Vlahović, I. & Tišljar, J. (Eds.): Evolution of Depositional Environments from the Paleozoic to the Quaternary in the Karst Dinarides and the Pannonian Basin. 22nd IAS Meeting of Sedimentology, Opatija–September 17–19, 2003, Field Trip Guidebook, 155–161.

Pavelić D., Kovačić M., Tibljaš D. Galić I., Marković F. & Pavičić I. 2022: The transition from a closed to an open lake in the Pannonian Basin System (Croatia) during the Miocene Climatic Optimum: Sedimentological evidence of Early Miocene regional aridity, *Palaeogeography, Palaeoclimatology, Palaeoecology* 586, 110786. https://doi.org/10.1016/j.palaeo.2021.110786

Pearce J.A. 1982: Trace element characteristics of lavas from destructive plate boundaries. In: Thorpe,R.S. (Ed.): Andesites. *Wiley*, New York, 525–548.

Pécskay Z., Lexa J., Szakács A., Balogh K., Seghedi I., Konečný V., Kovacs M., Márton E., Kaličiak M., Széky-Fux V., Póka T., Gyarmati P., Edelstein O., Rosu E. & Žec B. 1995: Space and time distribution of Neogene-Quaternary volcanism in the Carpatho-Pannonian region. *Acta Vulcanologica* 7, 15–28.

Pécskay Z., Lexa J., Szakács A., Seghedi I., Balogh K., Konečný V., Zelenka T., Kovacs M, Póka T., Fülöp A., Márton E., Panaiotu C. & Cvetković V. 2006: Geochronology of Neogene magmatism in the Carpathian arc and intra-Carpathian area. *Geologica Carpathica* 57, 511–530.

Perch-Nielsen K. 1985: Cenozoic calcareous nannofossils. In: Bolli H.M., Saunders J.B. & Perch-Nielsen K. (Eds): Plankton Stratigraphy. *Cambridge University Press*, Cambridge, 1–454.

Peryt D., Garecka M. & Peryt T.M. 2021: Foraminiferal and calcareous nannoplankton biostratigraphy of the upper Badenian–lower Sarmatian Strata in the SE Polish Carpathian foredeep. *Geological Quarterly* 65, 18. https://doi.org/10.7306/gq.1584

Püspöki Z., Kozák M., Kovács-Pálffy P., Földvári M., Mcintosh L.W. & Vincze L. 2005: Eustatic and tectonic/volcanic control in sedimentary bentonite formation - a case study of Miocene bentonite deposits from the Pannonian Basin. *Clays and Clay Minerals* 53, 71–91. https://doi.org/10.1346/CCMN.2005.0530108

Püspöki Z., Kozák M., Kovács-Pálffy P., Szepesi J., Mcintosh R., Kónya P., Vincze L. & Gyula G. 2008: Geochemical records of a bentonitic acid-tuff succession related to a transgressive systems tract – Indication of changes in the volcanic sedimentation rate. *Clays Clay Minerals* 56, 23–38. https://doi.org/10.1346/CCMN.2008.0560103

Rao P.C. 1996: Modern carbonates, tropical, temperate, polar. Introduction to sedimentology and geochemistry. *University of Tasmania*, Tasmania, 1–206.

Rögl F. 1996: Stratigraphic correlation of the Paratethys Oligocene and Miocene. *Mitteilungen der Gesellschaft der Geologie- und Bergbaustudenten* 41, 65–73.

Rosu E., Pécskay Z., Stefan A., Popescu G., Panaiotu C. & Panaiotu C.E. 1997: The Evolution of the Neogene volcanism in the Apuseni Mountains (Rumania): constraints from new K-Ar data. *Geologica Carpathica* 48, 353–359.

Rosu E., Seghedi I., Downes H., Alderton D.H.M., Szakács A., Pécskay Z., Panaiotu C., Panaiotu C E. & Nedelcu L. 2004:

Extension-related Miocene calc-alkaline magmatism in the Apuseni Mountains, Romania: Origin of magmas. *Swiss Bulletin of Mineralogy and Petrology* 84, 153–172.

Royden L.H. 1988: Late Cenozoic Tectonics of the Pannonian Basin System. In: Royden L.H. & Horvath I.F. (Eds.): The Pannonian Basin. A study in Basin Evolution. *AAPG Memoir Tulsa* 45, 27–48.

Ruman A. 2017: Reflection of tectonics and change of the depositional environment and Danube basin palaeogeography in the paleoecology of foraminifers, PhD Thesis, *Comenius university in Bratislava, Faculty of natural sciences*, 1–112.

Rybár S., Šarinová K., Sant K., Kuiper K.F., Kováčová M., Vojtko R., Reiser M.K., Fordinál K., Teodoridis V., Nováková P.& Vlček T. 2019: New $^{40}Ar/^{39}Ar$, fission track and sedimentological data on a middle Miocene tuff occurring in the Vienna Basin: Implications for the north-western Central Paratethys region. *Geologica Carpathica* 70, 386–404. https://doi.org/10.2478/geoca-2019-0022

Schultz L.G. 1964: Quantitative interpretation of mineralogical composition from X-ray and chemical data for the Pierre Shale. *U.S. Geological Survey Professional Paper* 39 (1C), 1–31.

Seghedi I. & Downes H. 2011: Geochemistry and tectonic development of Cenozoic magmatism in the Carpathian–Pannonian region. *Gondwana Research* 20, 655–672. https://doi.org/10.1016/j.gr.2011.06.009

Seghedi I., Downes H., Harangi S., Mason P.R.D. & Pécskay Z. 2005: Geochemical response of magmas to Neogene–Quaternary continental collision in the Carpathian–Pannonian region: A review. *Tectonophysics* 410, 485–499. https://doi.org/10.1016/j.tecto.2004.09.015

Slovenec D. & Šegvić B. 2021: Middle Triassic high-K calc-alkaline effusive and pyroclastic rocks from the Zagorje-Mid-Transdanubian Zone (Mt. Kuna Gora; NW Croatia): mineralogy, petrology, geochemistry and tectono-magmatic affinity. *Geologica Acta* 19.2, 1–23. https://doi.org/10.1344/geologicaacta2021.19.2

Starkey H.C., Blackmon P.D. & Hauff P.L. 1984: The Routine Mineralogical Analysis of Clay-Bearing Samples. *U.S. Geological Survey Bulletin* 1563, 1–31.

Steininger F.F., Müller C. & Rögl F. 1988: Correlation of Central Paratethys, Eastern Paratethys, and Mediterranean Neogene Stages. In: Royden L.H. & Horvath F. (Eds.): The Pannonian Basins. A study in Basin Evolution. *AAPG Memoir* 45, 79–87.

Sun S. & McDonough W.F. 1989: Chemical and isotopic systematics of oceanic basalts: implications for mantle composition and processes. *Geological Society, London, Special Publications* 42, 313–345. https://doi.org/10.1144/GSL.SP.1989.042.01.19

Szakács A., Pécskay Z. & Gál A. 2018: Patterns and trends of time–space evolution of Neogene volcanism in the Carpathian–Pannonian region: a review. *Acta Geodaetica et Geophysica* 53, 347–367. https://doi.org/10.1007/s40328-018-0230-3

Szczechura J. 2000: Age and evolution of depositional environments of the supra- evaporitic deposits in the northern, marginal part of the Carpathian Foredeep: micropalaeontological evidence. *Geological Quarterly* 44, 81–100.

Szuromi-Korecz A., Magyar I., Sztanó O., Csoma V., Botka D., Sebe K. & Tóth E. 2021: Various marginal marine environments in the Central Paratethys: Late Badenian and Sarmatian (middle Miocene) marine and non-marine microfossils from Pécs-Danitzpuszta, southern Hungary. *Földtani Közlöny* 151, 275–305. https://doi.org/10.23928/foldt.kozl.2021.151.3.275

Šimunić A. & Pamić J. 1993: Geology and petrology of Egerian–Eggenburgian andesites from the easternmost parts of the Periadriatic Zone in Hrvatsko Zagorje (Croatia). *Acta Geologica Hungarica* 36, 315–330.

Šimunić An., Pikija M., Hećimović I. & Šimunić Al. 1981: Basic Geological Map of SFRY 1:100000, Geology of the Varaždin sheet L 33-69. *Institut za geološka istraživanja*, Zagreb, *Savezni geološki zavod*, Beograd, 1–75 (in Croatian).

Šimunić An., Pikija M. & Hećimović I. 1982: Basic Geological Map of SFRY 1:100000, Varaždin sheet L 33-69). *Institut za geološka istraživanja*, Zagreb, *Savezni geološki zavod*, Beograd (in Croatian).

Tappan H. 1980: The paleobiology of plant protists. *W.H. Freeman and Company*, San Francisco, 1–1028.

Tari G., Horváth F. & Rumpler J. 1992: Styles of extension in the Pannonian Basin. *Tectonophisics* 208, 203–219. https://doi.org/10.1016/B978-0-444-89912-5.50016-8

Taylor S.R. & McLennan S.M. 1985: The Continental Crust: Its composition and evolution. *Blackwell*, Oxford, 1–312.

Tibljaš D., Loparić V. & Belak M. 2002: Discriminant function analysis of Miocene volcaniclastic rocks from North-Western Croatia based on geochemical data. *Geologia Croatica* 55, 39–44. https://doi.org/10.4154/GC.2002.04

Tišljar J 2001: Sedimentology of carbonates and evaporites (in Croatian). *Institut za geološka istraživanja*, 1–375 (in Croatian).

Tóth E. & Görög Á. 2008: Sarmatian foraminifera fauna from Budapest (Hungary). *Hantkeniana* 6, 187–217.

Tribovillard N., Algeo T. J., Baudin F. & Riboulleau A. 2012: Analysis of marine environmental conditions based on molybdenum – uranium covariation — Applications to Mesozoic paleoceanography. *Chemical Geology* 324, 46–58. https://doi.org/10.1016/j.chemgeo.2011.09.009

Tyson R.V. 1995: Sedimentary Organic Matter. Organic Facies and Palynofacies. *Chapman and Hall*, London, 1–615.

Uffenorde H. 1972: Ökologie und jahrszeitliche Verteilung rezenter benthonischer Ostracoden des Limski Kanal bei Rovinj (nördliche Adria). *Göttinger Arbeiten zur Geologie und Paläontologie* 13, 1–121.

Van de Wal R.S.W., De Boer B., Lourens L.J., Köhler P. & Bintanja R. 2011: Reconstruction of a continuous high-resolution CO_2 record over the past 20 million years. *Climate of the Past* 7, 1459–1469. https://doi.org/10.5194/cp-7-1459-2011

Van Morkhoven F.P.C.M. 1963: Post-Palaeozoic Ostracoda. Their morphology, taxonomy and economic use. Vol. II. Generic Descriptions. *Elsevier Publ. Co.*, Amsterdam, London, New York, 1–478.

Vlček T., Šarinová K., Rybár S., Hudáčková N., Jamrich M., Šujan M., Franců J., Nováková P., Sliva Ľ., Kováč M. & Kováčová M. 2020: Paleoenvironmental evolution of Central Paratethys Sea and Lake Pannon during the Cenozoic. *Palaeogeography, Palaeoclimatology, Palaeoecology* 559, 109892. https://doi.org/10.1016/j.palaeo.2020.109892

Vrabac S., Ćorić S., Đulović Z. & Ječmenica I. 2015: Discordance between the Badenian and the Sarmatian in the procile Spasine near Ugljevik (in Bosnian). In: Skopljak F. (Ed.): Zbornik radova: knjiga sažetaka 1. Kongres geologa u Bosni i Hercegovini sa međunarodnim učešćem, Tuzla, 21-23. 10, 10–15.

Vrsaljko D. 1999: The Pannonian Palaeoecology and Biostratigraphy of Molluscs from Kostanjek - Medvednica Mt., Croatia. *Geologia Croatica* 52, 9–27. https://doi.org/10.4154/GC.1999.02

Vrsaljko D., Pavelić D., Miknić M., Brkić B., Kovačić M., Hećimović I., Hajek-Tadesse V., Avanić R. & Kurtanjek N. 2006: Middle Miocene (Upper Badenian/Sarmatian) Palaeoecology and Evolution of the Environments in the Area of Medvednica Mt. (North Croatia). *Geologia Croatica* 59, 51–63. https://doi.org/10.4154/GC.2006.04

Weaver C.E. 1989: Clays, Muds, and Shales. *Elsevier*, Amsterdam, 1–721.

Wei W. & Algeo T.J. 2019: Elemental proxies for paleosalinity analysis of ancient shales and mudrocks. *Geochimica et Cosmochimica Acta* 287, 341–366. https://doi.org/10.1016/j.gca.2019.06.034

Wilson M.J. 2004: Weathering of the primary rock-forming minerals: processes, products and rates. *Clay Minerals* 39, 233–266. https://doi:10.1180/0009855043930133

Winchester J.A. & Floyd P.A. 1977: Geochemical discrimination of different magma series and their differentiation products using immobile elements. *Chemical Geology* 20, 325–343.

Wood G.D., Gabriel A.M. & Lawson J.C. 1996: Palynological techniques: processing and microscopy. In: Jansonius J. & McGregor D.C. (Eds.): Palynology: Principles and Applications. *American Association of Stratigraphic Palynologists Foundation* 1, 29–50.

Zlinská A., Hudáčková N. & Koubová I. 2010: Lower Sarmatian Foraminifera from marginal marine environments in the Malacky Vicinity (Vienna Basin). Geologické výzkumy na Moravě a ve Slezsku. 17, 1–2, 16th Conference on Upper Tertiary, Brno, 104–106.

Žvab Rožič P., Vidović J., Ćosović V., Hlebec A., Rožič B. & Dolenec M. 2022: A Multiparametric Approach to Unravelling the Geoenvironmental Conditions in Sediments of Bay of Koper (NE Adriatic Sea): Indicators of Benthic Foraminifera and Geochemistry. *Frontiers in Marine Science* 9, 1–18. https://doi.org/10.3389/fmars.2022.812622

Electronic supplementary material is available online:

Supplement 1 at http://geologicacarpathica.com/data/files/supplements/GC-74-1-Grizelj_Suppl1.xlsx
Supplement 2 at http://geologicacarpathica.com/data/files/supplements/GC-74-1-Grizelj_Suppl2.xlsx
Supplement 3 at http://geologicacarpathica.com/data/files/supplements/GC-74-1-Grizelj_Suppl3.xlsx
Supplement 4 at http://geologicacarpathica.com/data/files/supplements/GC-74-1-Grizelj_Suppl4.xlsx
Supplement 5 at http://geologicacarpathica.com/data/files/supplements/GC-74-1-Grizelj_Suppl5.xlsx